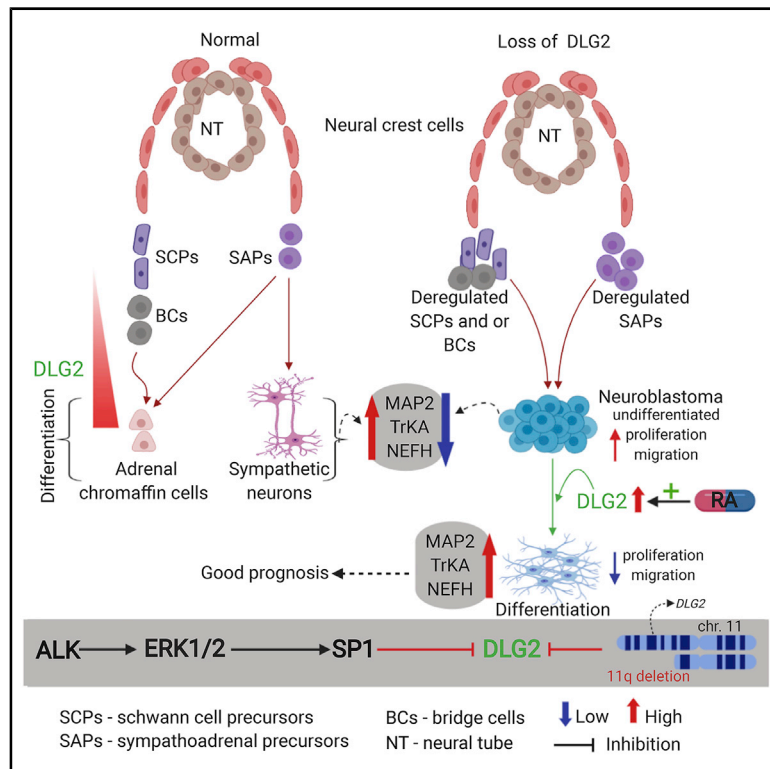# 11q Deletion or ALK Activity Curbs DLG2 Expression to Maintain an Undifferentiated State in Neuroblastoma

Graphical Abstract

Authors

Joachim Tetteh Siaw, Niloufar Javanmardi, Jimmy Van den Eynden, ..., Ruth H. Palmer, Bengt Hallberg, Tommy Martinsson

Correspondence

ruth.palmer@gu.se (R.H.P.), bengt.hallberg@gu.se (B.H.), tommy.martinsson@gu.se (T.M.)

In Brief

Siaw et al. show that oncogenic ALK-ERK1/2-SP1 signaling maintains neuroblastoma cells in an undifferentiated state through the suppression of *DLG2* transcription. The expression of *DLG2* drives differentiation and inhibits tumor growth. Genetic analysis of high-risk 11q deletion neuroblastoma identifies genetic lesions in the *DLG2* gene in patient samples.

Highlights

- ALK-ERK-SP1 signaling promotes an undifferentiated state in neuroblastoma cells

- ALK signaling suppresses DLG2 transcription

- DLG2 expression drives differentiation of neuroblastoma cells

- 11q deletion neuroblastomas exhibit genetic lesions in the *DLG2* locus

Cell Reports

Article

11q Deletion or ALK Activity Curbs DLG2 Expression to Maintain an Undifferentiated State in Neuroblastoma

Joachim Tetteh Siaw,[1,10] Niloufar Javanmardi,[2,10] Jimmy Van den Eynden,[3,10] Dan Emil Lind,[1] Susanne Fransson,[2] Angela Martinez-Monleon,[2] Anna Djos,[2] Rose-Marie Sjöberg,[2] Malin Östensson,[4] Helena Carén,[5] Gunhild Trøen,[6,7] Klaus Beiske,[6,7] Ana P. Berbegall,[8] Rosa Noguera,[8] Wei-Yun Lai,[1] Per Kogner,[9] Ruth H. Palmer,[1,11,*] Bengt Hallberg,[1,11,12,*] and Tommy Martinsson[2,11,*]

[1]Department of Medical Biochemistry and Cell Biology, Institute of Biomedicine, Sahlgrenska Academy, University of Gothenburg, 40530 Gothenburg, Sweden
[2]Department of Laboratory Medicine, Institute of Biomedicine, Sahlgrenska Academy, University of Gothenburg, Gothenburg, 40530 Gothenburg, Sweden
[3]Department of Human Structure and Repair, Anatomy and Embryology Unit, Ghent University, 9000 Ghent, Belgium
[4]Bioinformatics Core Facility, Sahlgrenska Academy, University of Gothenburg, 40530 Gothenburg, Sweden
[5]Sahlgrenska Center for Cancer Research, Department of Laboratory Medicine, Institute of Biomedicine, Sahlgrenska Academy, University of Gothenburg, Gothenburg, Sweden
[6]Institute of Clinical Medicine, University of Oslo, Oslo, Norway
[7]Department of Pathology, Oslo University Hospital, Oslo, Norway
[8]Department of Pathology, Medical School, University of Valencia/INCLIVA, Valencia/CIBER of Cancer, Madrid, Spain
[9]Childhood Cancer Research Unit, Department of Women's and Children's Health, Karolinska Institutet, Stockholm, Sweden
[10]These authors contributed equally
[11]Senior authors
[12]Lead Contact
*Correspondence: ruth.palmer@gu.se (R.H.P.), bengt.hallberg@gu.se (B.H.), tommy.martinsson@gu.se (T.M.)
https://doi.org/10.1016/j.celrep.2020.108171

SUMMARY

High-risk neuroblastomas typically display an undifferentiated or poorly differentiated morphology. It is therefore vital to understand molecular mechanisms that block the differentiation process. We identify an important role for oncogenic ALK-ERK1/2-SP1 signaling in the maintenance of undifferentiated neural crest-derived progenitors through the repression of DLG2, a candidate tumor suppressor gene in neuroblastoma. *DLG2* is expressed in the murine "bridge signature" that represents the transcriptional transition state when neural crest cells or Schwann cell precursors differentiate to chromaffin cells of the adrenal gland. We show that the restoration of DLG2 expression spontaneously drives neuroblastoma cell differentiation, highlighting the importance of DLG2 in this process. These findings are supported by genetic analyses of high-risk 11q deletion neuroblastomas, which identified genetic lesions in the *DLG2* gene. Our data also suggest that further exploration of other bridge genes may help elucidate the mechanisms underlying the differentiation of NC-derived progenitors and their contribution to neuroblastomas.

INTRODUCTION

Pediatric neuroblastoma (NB) is a heterogeneous disease, with differing prognosis depending on the subgroup. Some cases undergo spontaneous differentiation or regression with little or no therapy, while cases classified as high-risk NB have a decreased response rate to standard therapeutic regimens and relapse with an overall survival rate of <40% at 5 years (Maris, 2010; Maris et al., 2007). NB is characterized by multiple somatic chromosomal lesions at the genetic level, including structural variations (SVs) and copy-number alterations (CNAs). Relatively few mutations are detected in NB in comparison to other cancer types (De Brouwer et al., 2010; Gröbner et al., 2018; Pugh et al., 2013). The common

genetic features of NB include deletion of chromosome arm 1p, gain of parts of 17q, aneuploidy and amplification of the proto-oncogene *MYCN*, and deletion of parts of chromosome arm 11q, which are used to distinguish between high- and low-risk NB (Brodeur, 2003; Carén et al., 2008, 2010; De Brouwer et al., 2010; Hoehner et al., 1996; Maris, 2010; Park et al., 2013; Pugh et al., 2013). Previous studies have reported 11q deletions (11q del) in 43% of cases, suggesting this to be the most common deletion observed in NB tumors. Although unbalanced chromosomal alterations affecting 11q have been known for some time, no single candidate gene has been confirmed to play a role in NB despite intensive investigation, including thorough deletion mapping of this crucial region (11q14–q24) (Carén et al., 2008, 2010; Srivatsan et al., 1993).
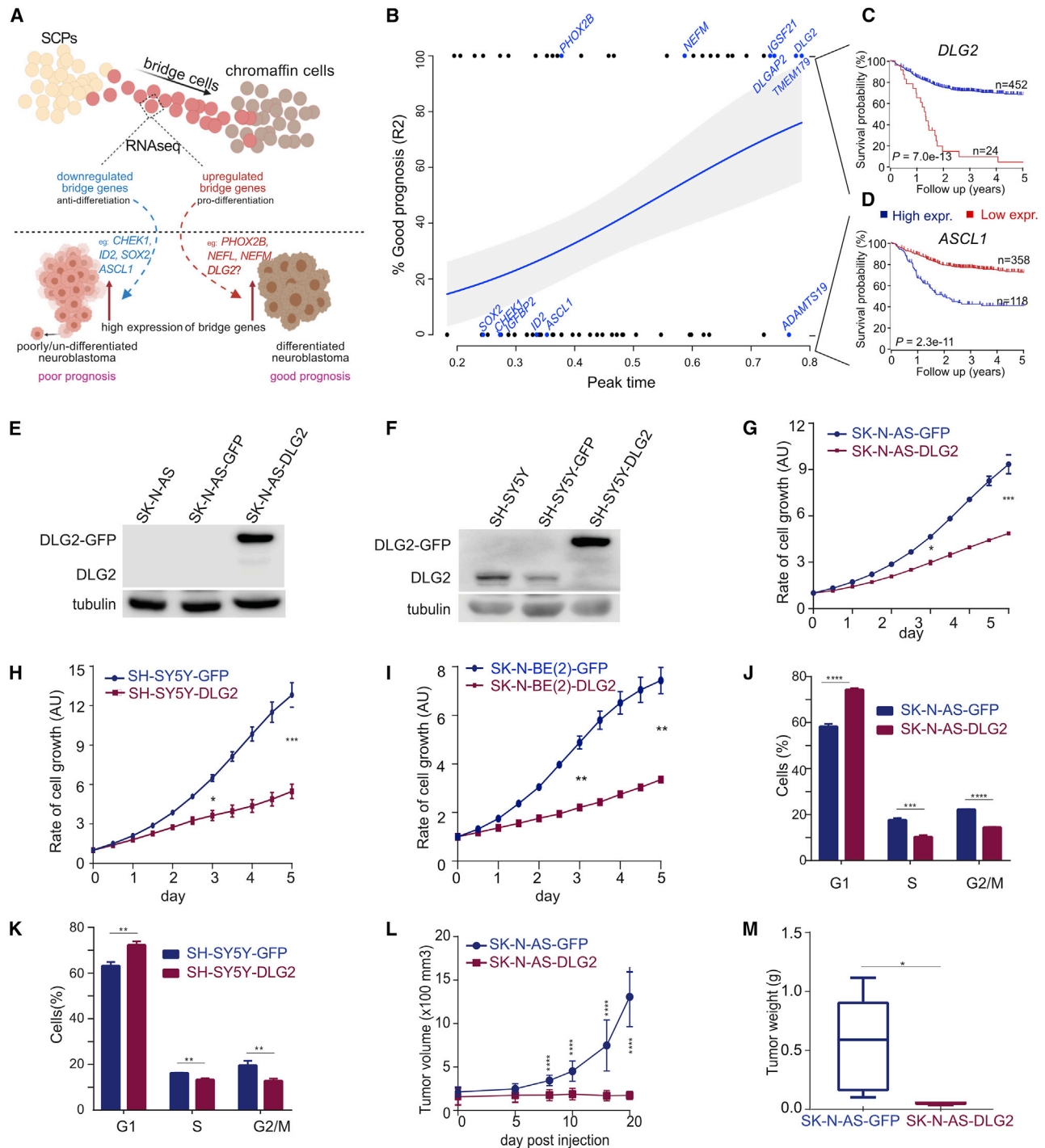
Figure 1. The Bridge Gene *DLG2* Suppresses NB Tumorigenic Growth

(A) Schematic overview of the transcription-based hypothesis outlining the differentiation trajectory of SCPs toward adrenal chromaffin fate (Furlan et al., 2017). SCPs, Schwann cell precursors (yellow); bridge cells (red), chromaffin cells (brown).

(B–D) Logistic regression analysis of the expected effect of bridge gene expression on prognosis as a function of peak expression pseudotime (B). The graph shows a regression line, with the 95% confidence interval indicated by the gray area. The dots represent bridge genes with either a positive (upper dots) or a negative (lower dots) correlation between expression and prognosis, as derived from the R2 platform (Kocak dataset, KaplanScan method) and illustrated (C) for *DLG2* and (D) *ASCL1* by the survival plots on the right. The bridge gene and pseudotime data were derived from Furlan et al. (2017). Only bridge genes that were unambiguously mapped from mouse to human gene names were used for the analysis.

(E and F) Western blot confirmation of DLG2-GFP overexpression in SK-N-AS and SH-SY5Y cells.

(legend continued on next page)

In recent years, our understanding of the underlying developmental processes involved in NB has increased. NB is considered an embryonal malignancy of the sympathetic nervous system that develops from un-differentiated neural crest-derived cells (NCCs), arising in the adrenal medulla and the sympathetic ganglia (Huber et al., 2009; Saito et al., 2012). NCCs arise at mid-gestation around the closure of the neural tube. Subsequently, NCCs undergo migration, ultimately generating a variety of tissues. In the sympathoadrenal (SA) lineage, NCCs reach their destinations close to the dorsal aorta, where they proliferate, differentiate into neurons and glia, and finally form the sympathetic ganglia and the chromaffin cells that contribute to the adrenal medulla. Recently, it was reported that the majority of chromaffin cells in the adrenal medulla arise from peripheral stem cells called Schwann cell precursors (SCPs) (Furlan et al., 2017). SCPs migrate along the visceral motor nerves to the vicinity of the developing adrenal gland and form postsynaptic neuroendocrine chromaffin cells.

During development, the adrenal medulla is thought to be generated from both neural crest SA lineage cell precursors and SCPs, with SA lineage cell precursors destined to become sympathetic neurons or chromaffin cells and SCPs destined to become chromaffin cells (Furlan et al., 2017). In their study, Furlan and coworkers examined the transcriptional transition from SCPs to chromaffin cells and revealed a transient cellular state connecting both SCPs and chromaffin cells, identifiable by a transcriptional pattern, which they called the bridge signature. In this signature, they identified SCP-specific genes that were downregulated and upregulated in cells undergoing differentiation to an adrenergic (ADRN) chromaffin fate (Furlan et al., 2017). Loss of differentiation is a hallmark of high-risk NB, and loss of key differentiation factors potentially affect NB progression, highlighted by the presence of PHOX2B in the bridge signature. Furthermore, there are well-established genetic mutations in several loci that are associated with development of NB, including ALK, PTPN11, and ATRX (Pugh et al., 2013). Recently, it was observed that the expression of ALK-F1174L gain-of-function mutation during embryogenesis impairs the differentiation of neural crest progenitors in sympathetic ganglia (Vivancos Stalin et al., 2019). In addition, NB tumors with evidence of high ALK or MYCN protein expression exhibit undifferentiated or poorly differentiated histology (Chang et al., 2020). Since many cases of low-risk NB either differentiate or regress, there is much interest in identifying differentiation-inducing mechanisms for NB. One identified factor that induces differentiation is retinoic acid (RA), which is used clinically and improves event-free survival (Brodeur and Bagatell, 2014; de Thé, 2018; Matthay et al., 1999).

Based on our current understanding of NB, we hypothesized that genes included in the bridge signature may contribute to NB progression. To understand this better, we investigated the relationship between the expression of the individual bridge genes and NB prognosis. This in silico analysis also suggested the Disks Large Homolog 2 (DLG2) gene as a strong candidate that may play a role in differentiation in an NB context. Subsequent biochemical, in vitro, and in vivo analyses identified DLG2 protein as a critical determinant of differentiation in NB cells. When combined with differentiation-promoting factors such as RA or nerve growth factor (NGF), DLG2 expression resulted in almost complete differentiation of NB cells. In keeping with this function, we also show that DLG2 levels are highly sensitive to ALK pathway activity, and in differentiation-poor ALK-driven NB DLG2 expression is suppressed, allowing ALK to promote an undifferentiated NB state. A role for DLG2 as a tumor suppressor gene is supported by genetic analysis of NB patient material that identifies genetic lesions at 11q mapping at high frequency to the DLG2 gene. Our results identify DLG2 as a tumor suppressor in NB that plays a critical role in the differentiation of neural crest lineages.

RESULTS

Genes Expressed during SCP to Chromaffin Cell Differentiation Are Prognostic of NB Patient Outcome
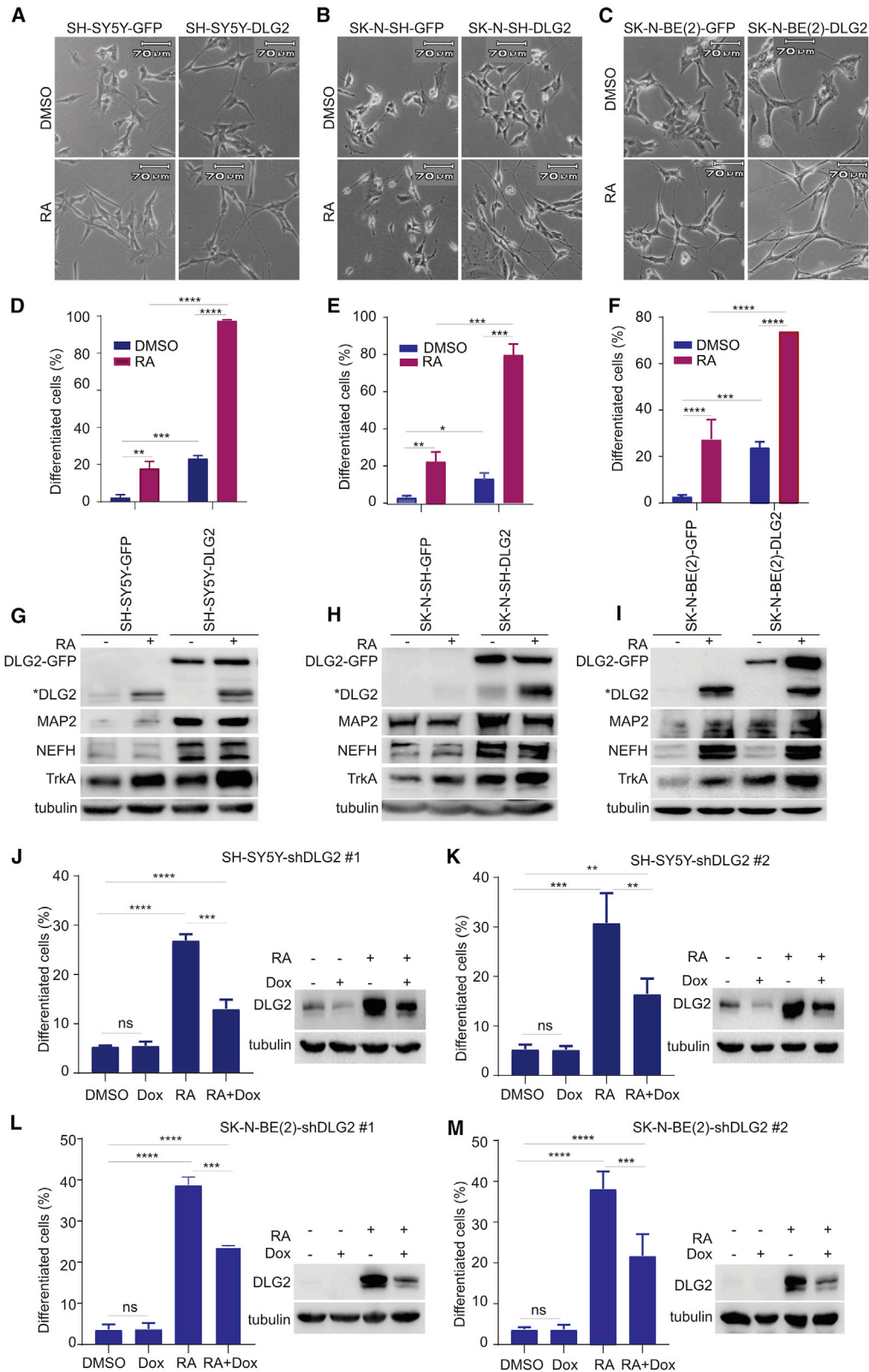
NB is considered a disease of failed differentiation of neural crest-derived progenitors such as SCPs and sympathoadrenal precursor cells. Furlan et al. (2017) identified a unique set of murine genes expressed by transient intermediate cells they called bridge cells that arise during the differentiation of SCPs to adrenal chromaffin cells (Figure 1A). Since ~50% of NB arises in the adrenal gland, we hypothesized that the deregulation of genes and signaling pathways in the bridge cells could block progenitor cell differentiation. We further hypothesized that genes that are uniquely downregulated or upregulated in the bridge cells could be anti- or pro-differentiation, respectively (Figure 1A). Hence, high expression of genes that are up- or downregulated in the bridge cells may promote undifferentiated (poor prognosis) or differentiated (good prognosis) NB phenotypes, respectively (Figure 1A). To examine whether the temporal order of this regulation of murine bridge cell genes is associated with human NB tumor biology and patient outcome, we used the R2:genomics analysis and visualization platform (https://hgserver1.amc.nl:443/) to investigate their correlation with NB prognosis (Kocak NB dataset; 649 tumors). The high overall expression of early peak time bridge cell genes in NB patient tumor material strongly correlated with poor prognosis, while high expression of late peak time bridge cell genes correlated with better prognosis (logistic regression p = 0.0019; Figures 1B–1D). A number of these genes have already been reported to play roles in NB pathogenesis, such as ASCL1 (Figure 1D) (Kasim et al., 2016), PHOX2B

(legend on next page)

(Trochet et al., 2004), *CHEK1* (Cole et al., 2011), *NEFM* (Murillo et al., 2017), *SOX2* (Yang et al., 2015), *IGFBP2* (Russo et al., 2005), and *ID2* (Wieczorek and Balwierz, 2015). However, many genes from the bridge cell signature, including *DLGAP2*, *IGSF21*, *ADAMTS19*, *DLG2*, and *TMEM179*, are regulated in the developmental timeline toward the chromaffin phenotype and have not been functionally investigated in NB. We hypothesized that the deregulation of these genes may play a role in NB progression.

Two genes of particular interest were *DLG2* and *DLGAP2*. The latter encodes a protein that has been shown to interact with DLG2 (Marshall et al., 2008). Earlier observations indicate that both DLG2 and DLGAP2 play a role in the molecular organization of synapse and neuronal signaling (Marshall et al., 2008). In the bridge signature, *DLG2* and *DLGAP2* are upregulated in the final steps of SCP to chromaffin cell differentiation (Figure 1B) (Furlan et al., 2017).

The *DLG2* gene encodes postsynaptic density protein 93 (PSD93), a protein belonging to the family of molecular scaffolding proteins known as membrane-associated guanylate kinases, or MAGUKs. A core of three disparate domains, including a guanylate kinase domain, an SH3 domain, and three PDZ domains interacting with each other, defines members of this protein family (Roberts et al., 2012). The *DLG2* homolog in *Drosophila*, *Dlg*, is a well-characterized tumor suppressor, which, when mutated, results in neoplastic overgrowth of the *Drosophila* imaginal discs (Woods and Bryant, 1991). Recently, *DLG2* has been reported as a tumor suppressor in both dog and human osteosarcomas (Shao et al., 2019). High *DLG2* levels correlate with better prognosis and event-free survival in NB patients (https://hgserver1.amc.nl:443/). This correlation was observed in four different NB patient datasets, using two different cutoff methods (Figures 1C and S1). *DLG2* lies on chromosome 11q, which is widely known as a high-risk deletion region in NB (Carén et al., 2008, 2010; Fieuw et al., 2012; Maris et al., 2001; Spitz et al., 2003; Srivatsan et al., 1993). Since a role for DLG2 in NB has not been described, we decided to investigate (1) its importance in the differentiation of NB cells and (2) the putative tumor suppression function of DLG2 in NB.

DLG2 Overexpression Potently Inhibits Tumorigenic Phenotypes of NB Cells *In Vitro*

To investigate whether restoring DLG2 expression affected the tumorigenic properties of NB cells, we established stable, constitutive DLG2 expression in SK-N-AS, SH-SY5Y, and SK-N-BE(2) NB cell lines using a lentivirus-based expression system (Figures 1E, 1F, and S2F). The SK-N-AS cell line harbors an $NRAS^{Q61R}$ mutation with an 11q-deletion, SH-SY5Y harbors an

ALK^{F1174L} mutation together with chromosome 2p-gain, and SK-N-BE(2) harbors *MYCN* amplification together with a $p53^{C145F}$ mutation and low *NF1* expression. DLG2 expression in SK-N-AS-DLG2, SH-SY5Y-DLG2, and SK-N-BE(2)-DLG2 cells significantly inhibited cell proliferation *in vitro* (***p < 0.001, Figures 1G–1I) and induced G1 cell-cycle arrest (Figures 1J and 1K) in NB cells. Thus, in agreement with our hypothesis, the expression of DLG2 resulted in reduced cell growth.

DLG2 Inhibits Tumor Growth *In Vivo*

An important hallmark of a tumor suppressor is the ability to inhibit cell division and replication as an anti-oncogene. To determine whether our *in vitro* results were relevant in an *in vivo* NB model, we implanted SK-N-AS-DLG2 cells and SK-N-AS-GFP controls in nude mice and monitored tumor xenograft growth over time. DLG2 expression robustly impaired the growth of SK-N-AS-DLG2 xenografts relative to SK-N-AS-GFP controls, with a significant difference between tumor weight and volume at 20 days post-injection (****p < 0.0001, *p < 0.05, Figures 1L and 1M). These results support our initial observations that DLG2 functions as a tumor suppressor in NB cells and are in agreement with recent observations in osteosarcomas (Shao et al., 2019) and work in *Drosophila* (Woods and Bryant, 1991).

Ectopic DLG2 Expression Drives Neuronal Differentiation

We next investigated a role for DLG2 in neuronal differentiation, using neurite outgrowth as a readout for differentiation. SH-SY-5Y, SK-N-SH, and SK-N-BE(2) NB cells overexpressing DLG2 displayed increased neurite outgrowth when compared with GFP controls (Figures 2A–2F and S2). In addition, cells overexpressing DLG2 exhibited an upregulation of established neuronal lineage differentiation markers, such as MAP2A, NEFH, and TRKA (Cheung et al., 2009; Chu et al., 2003) (Figures 2G–2I and S2).

From a clinical point of view, NB tumors with well-differentiated phenotypes are associated with better prognoses (He et al., 2017). RA, a differentiation agent, has been shown to improve event-free survival in high-risk NB patients with minimal residual disease (Matthay et al., 1999, 2009). Presently, RA is used as a maintenance therapy in high-risk NB patients (Masetti et al., 2012). We therefore asked whether DLG2 plays a role in RA-induced differentiation. The expression of DLG2 in NB cells induced neuronal differentiation to ~20%, which is comparable to RA-treated GFP control cells (Figures 2A–2I). However, DLG2 expression robustly enhanced RA-induced NB differentiation, and >80% of cells differentiated within 24 h compared to RA-treated controls (Figures 2A–2F). Further analysis revealed

---

Figure 2. Ectopic DLG2 Expression Induces Neuronal Differentiation

(A–C) Representative images showing morphological differentiation of NB cells upon either DMSO or retinoic acid (RA) (10 μM) treatment for 24 h (for SH-SY5Y cells) or 48 h (for SK-N-SH and SK-N-BE(2) cells). SH-SY5Y (GFP or DLG2-GFP) (A), SK-N-SH (GFP or DLG2-GFP) (B), and SK-N-BE(2) (GFP or DLG2-GFP) (C).

(D–F) Bar charts showing percentage differentiation of respective NB cells following RA treatment.

(G–I) Western blot showing the effect of DLG2 overexpression and RA on expression of neuronal differentiation markers in the indicated NB cells. Asterisk (*) denotes the endogenous DLG2 protein.

(J–M) Effect of doxycycline (Dox)-inducible shRNA-mediated DLG2 knockdown in SH-SY5Y (J and K) and SK-N-BE(2) (L and M) on RA-induced differentiation of cells, as quantified in bar graphs. The western blots indicate the effect of inducible DLG2 shRNA on DLG2 protein expression upon the treatment of cells with DMSO or RA (10 μM), Dox (250 ng/mL), or a combination of RA and Dox.

Unpaired t test. **p < 0.01, ***p < 0.001, and ****p < 0.0001. Quantified data are means ± SDs of at least 3 independent experiments. Scale bar (A–C), 70 μM.

that RA treatment led to endogenous DLG2 protein expression (Figures 2G–2I). The expression of DLG2 together with RA stimulation induced almost complete differentiation of NB cells, a level of differentiation response that had not been observed previously (Kasim et al., 2016; Pandey et al., 2014).

DLG2 Is Required for RA-Induced Differentiation

Since the expression of DLG2 resulted in a robust differentiation response, we next asked whether the loss of DLG2 would affect the RA-induced differentiation response. To do this, we generated stable NB cell lines expressing doxycycline-inducible *DLG2* small hairpin (shRNA). Inducible DLG2 knockdown resulted in reduced DLG2 protein levels and inhibited RA-mediated neuronal differentiation in both *MYCN* amplified (SK-N-BE(2)) and non-*MYCN*-amplified (SH-SY5Y) cells (Figures 2J–2M). These results confirm that DLG2 is required for a complete RA-induced differentiation response in NB cells.

RA Transcriptionally Regulates *DLG2* Expression in NB Cells

To further understand these observations, we examined the effect of RA treatment on DLG2 in NB cells. RA treatment upregulates DLG2 expression in a time-dependent manner in SH-SY5Y, SK-N-SH, and SK-N-BE(2) cells (Figures S3A–S3C). Inhibition of transcription by the addition of actinomycin D blocked RA-induced DLG2 protein expression in SH-SY5Y cells (Figure S3D), suggesting that RA regulates DLG2 at the level of transcription. We confirmed this by qPCR analysis, in which *DLG2* mRNA was similarly upregulated in a time-dependent manner upon RA treatment (Figure S3E). As a positive control, we used *NTRK1* (encodes TRKA), a previously described bona fide RA transcription target (Figure S3F) (Lucarelli et al., 1995; von Holst et al., 1995). Thus, our observations indicate that RA regulates *DLG2* gene expression at the transcriptional level.

DLG2 Overexpression Potentiates NGF-Induced NB Cell Differentiation

In addition to RA induction of DLG2 levels, we noted an increased expression of TRKA (Figures S3A–S3C). Our earlier observations consistently identified upregulated TRKA protein expression in response to DLG2 expression in NB cells (Figures 2G–2I, S2B, S2D, and S2F). This was an interesting observation since low-risk NB patient tumors often exhibit the characteristic property of spontaneous differentiation and high TRKA expression levels (Hoehner et al., 1995). Furthermore, the overexpression of exogenous TRKA enhances NGF-induced differentiation in NB cell culture models (Emdal et al., 2015). Therefore, we examined the effect of NGF on DLG2-overexpressing cells. DLG2 expression resulted in the sensitization of NB cells to NGF-mediated morphological differentiation, increasing the percentage of neurite-bearing cells in both SH-SY5Y-DLG2 and SK-N-SH-DLG2 cells compared to their respective controls (Figures S4A–S4D). Since RA was able to drive DLG2 expression, we also examined the effect of NGF/TRKA signaling on DLG2 protein levels. Treatment of SH-SY5Y cells with NGF upregulated endogenous DLG2 protein expression in a time-dependent manner (Figure S4E). This suggests a positive feedback regulation between DLG2 and TrkA and further supports DLG2 as an integral component of the differentiation process.

DLG2 Promotes ADRN Identity in NB Cells

DLG2 expression during differentiation may play a key role in establishing the identity of neural crest cell and SCP progeny. To better understand the effect of DLG2 in NB biology, we determined the downstream transcriptional response of *DLG2* expression. Therefore, we performed RNA sequencing (RNA-seq) and compared differential expression between *DLG2*-overexpressing and control SH-SY5Y cells. *DLG2* overexpression resulted in 414 upregulated and 122 downregulated genes (differential expression defined at a log fold change (FC) cutoff of 2 at a 1% false discovery rate (FDR; Figure 3A). These differentially expressed genes were enriched for genes involved in neuronal differentiation (Figure 3B) and included the neuronal markers *NRCAM* ($\log_2$FC = 2.95), *NEFM* ($\log_2$FC = 2.69), *NEFH* ($\log_2$FC = 2.33), and *ASCL1* ($\log_2$FC = −3.85) (Figure 3A; Table S1). Similar responses were observed at the protein level (Figure S5; Table S1).

Because our previous results indicated similar neuronal differentiation effects between RA treatment and after *DLG2* overexpression, we compared the *DLG2*-induced gene expression changes with the transcriptional response resulting from the treatment of SH-SY5Y cells with RA for 24 h. RA treatment regulated 301 genes, with 83 (27.6%) of these overlapping with the response measured after *DLG2* overexpression and including *DLG2* itself ($\log_2$FC = 2.40; Table S1). The other genes were regulated by RA only and included *RET* ($\log_2$FC = 2.43), *MYC* ($\log_2$FC = −3.14), and *NTN4* ($\log_2$FC = 2.29). The neuronal differentiation markers *NRCAM*, *NEFM*, and *NEFH* were not significantly affected after RA treatment, with similar findings again between mRNA and protein levels (Table S1). Using hierarchical clustering, we identified a set of 73 genes that was uniquely upregulated by RA and was predicted to be regulated via the RA receptors *RARA* and *RARB* (cluster 2 in Figure 3C). A larger set of 263 genes was identified that responded to *DLG2* overexpression only and was predicted to be mediated by other transcription factors (TFs), such as *REST*, *SMAD1*, *TBP*, and *TCF4* (cluster 3 in Figure 3C). These results identify substantial transcriptional differences between *DLG2*-induced and RA-induced differentiation responses.

Since both ADRN and mesenchymal (MES) cell types have been reported in NB cells, we compared DLG- or RA-induced transcriptional responses to a published set of ADRN and MES signature genes. MES cells are enriched in post-therapy and relapsed NB tumors, resembling neural crest-derived precursor cells, which can differentiate into several types (van Groningen et al., 2017). Analysis of serial bone marrow samples in high-risk NB patients showed that MES mRNAs increase during treatment and were highly predictive of relapse (Wezel et al., 2019). In contrast, ADRN-type cells represent a more differentiated state, with similarities to the ADRN lineage as in chromaffin cells (van Groningen et al., 2017). ADRN mRNAs decrease during the treatment of NB patients, which may indicate the depletion of ADRN cells in the tumor (Wezel et al., 2019). An ADRN gene enrichment was observed for genes responding to *DLG2*
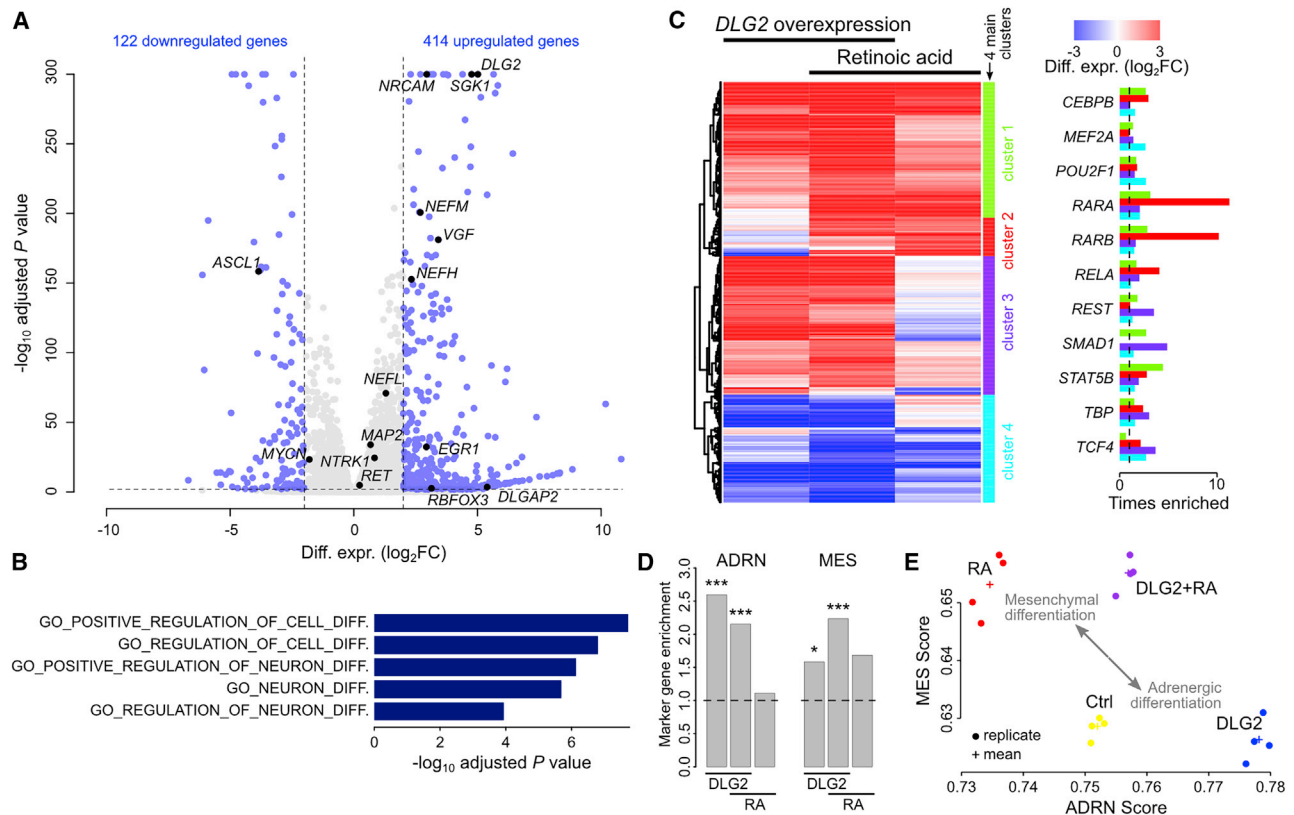
Figure 3. RNA-Seq Differential Expression Analysis of *DLG2* Overexpression

RNA-seq-based differential gene expression was measured in SH-SY5Y cells after overexpression of *DLG2*.

(A) Volcano plot with neuronal differentiation markers and *ASCL1* labeled in black. *DLG2* is also indicated in black. Dashed lines show differential expression cutoffs (log$_2$FC at 1% FDR).

(B) Gene Ontology (GO) gene set enrichment analysis (GSEA) on 536 differentially expressed genes. Bar plot shows the top 5 enriched GO terms related to differentiation.

(C) Heatmap comparing differential expression signatures between cells overexpressing *DLG2* and/or cells treated with RA for 24 h. Genes that are differentially expressed in minimal 1 condition are shown. Genes were hierarchically clustered, and the 4 main clusters are colored on the right side of the heatmap. The bar plot on the right shows the predicted transcription factors (TFs) responsible for each cluster, with indication of enrichment values.

(D) Bar plots indicate enrichments of ADRN (left) and MES (right) marker genes for different conditions, as indicated. *p < 0.05, **p < 0.01, and ***p < 0.001.

(E) MES and ADRN signature scores for cells in control conditions, overexpressing *DLG2* and/or treated with RA. Two-headed arrow indicates the 2-dimensional spatial difference between RA-treated and DLG2-overexpressing cells.

All of the experiments were performed using 4 biological replicates in each condition.

overexpression (2.6 times enriched, p = 4.3e−5, Fisher's exact test), but not for genes responding to RA treatment (p = 0.46; Figure 3D). A rank percentile-based scoring method has been suggested based on these gene signatures, in which MES differentiation is characterized by higher MES and lower ADRN scores and vice versa for ADRN differentiation (see van Groningen et al., 2017 and Method Details). We calculated these scores for our different experimental conditions and found ADRN scores after *DLG2* overexpression (mean 0.78 versus 0.75 in control conditions, p = 1.2e−6, Student's t test) and increased MES scores after RA treatment (mean 0.65 versus 0.63 in control conditions, p = 1.9e−5) (Figure 3E). In summary, our differential expression analysis suggested that *DLG2* expression results in a strong ADRN differentiation response, which is different from the more MES RA-induced differentiation response (Figures 3C–3E).

ALK Suppresses the Expression of DLG2 through the Mitogen-Activated Protein Kinase (MAPK) Pathway

Recently, we reported a clinical case in which an NB patient carrying an *ALK-I1171T* activating mutation was treated with the ALK inhibitor ceritinib. On resection after treatment, the residual primary tumor showed significant differentiation, resembling ganglioneuroblastoma (Guan et al., 2018). Expression of the human ALK-F1174L mutant in mouse neural crest cells significantly perturbs early sympathetic progenitor differentiation and increases their proliferation (Vivancos Stalin et al., 2019). While *ALK* mutations occur in ~10% of NB cases, Chang et al. (2020) recently reported high ALK protein expression in 41% of NB tumors, in which ~86% of tumors with high ALK or MYCN protein expression exhibited an undifferentiated or poorly differentiated histology. These reports highlight a potential effect of ALK signaling activity in maintaining a poorly differentiated NB state.
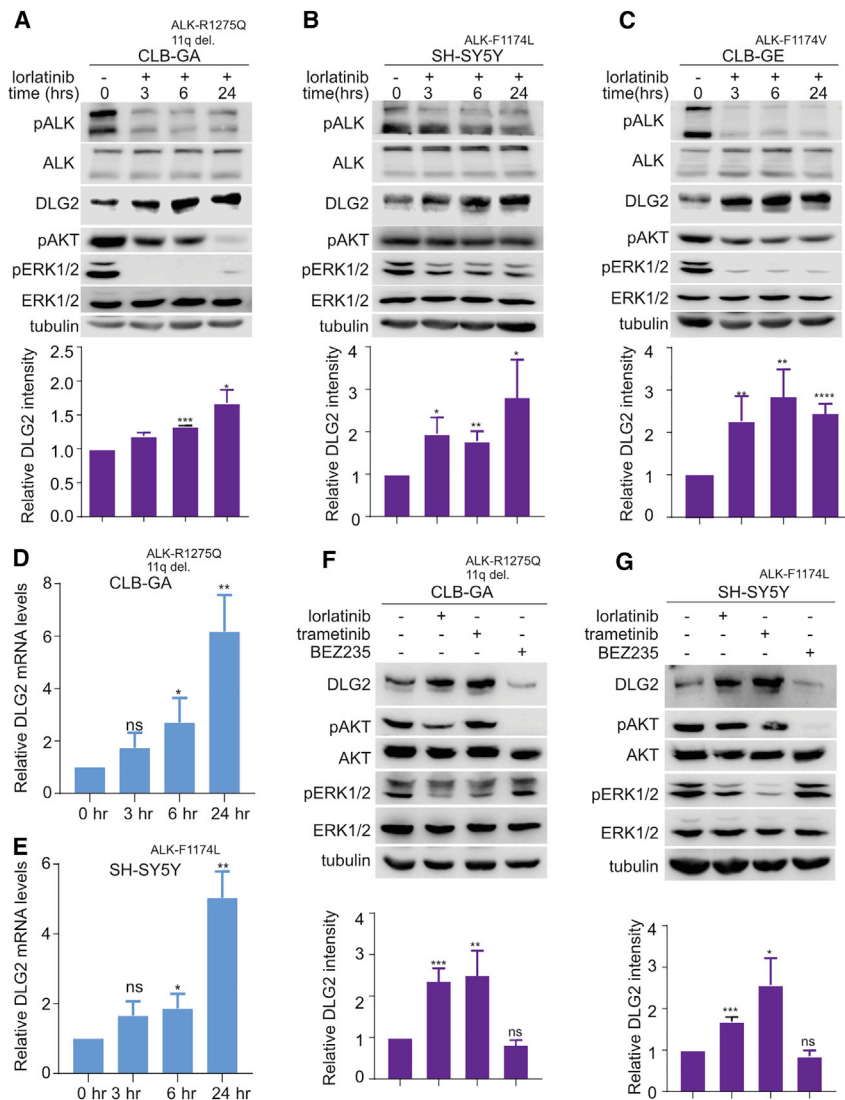
Figure 4. ALK Suppresses the Expression of DLG2 through the MAPK Pathway

(A–C) Western blot analyses of the effect of time-dependent ALK inhibition, with lorlatinib (30 nM), on DLG2 expression in the indicated NB cell lines.

(D and E) qPCR analyses of the effect of lorlatinib (30 nM) treatment on *DLG2* expression levels in the indicated NB cells.

(F and G) ALK-driven NB cells were treated with lorlatinib (30 nM), trametinib (10 nM), or BEZ235 (250 nM), and their effect on DLG2 protein levels determined by western blot analysis, quantified, and represented as bar graphs below. pAKT and pERK1/2 were included as readout for downstream signaling.

Unpaired t test. *p < 0.05, **p < 0.01, ***p < 0.001, and ****p < 0.0001; ns, not significant. Quantified data are means ± SDs of at least 3 independent experiments.

We next investigated the effect of ALK activity on DLG2 levels. Overall, NB cell lines express very low to undetectable DLG2 protein levels (Figure S6A). Treatment of ALK-dependent NB cells, such as CLB-GA, CLB-GE, and SH-SY5Y with the ALK tyrosine kinase inhibitor (TKI) lorlatinib, resulted in time-dependent upregulation of both DLG2 protein (Figures 4A–4C) and mRNA expression (Figures 4D and 4E). These results suggest that ALK signaling may transcriptionally repress expression of *DLG2* in NB.

As ALK signals through numerous downstream signaling pathways, including the MAPK and phosphatidylinositol 3-kinase (PI3K)-AKT pathways, we next determined the pathway by which ALK regulates DLG2. Inhibition of ERK1/2 downstream of ALK, with the MEK1/2 inhibitor (MEKi) trametinib increased DLG2 protein expression in a manner similar to that observed for ALK TKI treatment (Figures 4F and 4G). In agreement, trametinib treatment upregulated DLG2 protein expression in a time-dependent manner similar to ALK inhibi-

tor (ALKi) treatment (compare Figure S6B with Figures 4A–4C). In contrast, the inhibition of AKT activity with the PI3K inhibitor BEZ235 had no observable effect on DLG2 protein levels (Figures 4F and 4G). To highlight the importance of ERK signaling in the regulation of DLG2 expression, we also investigated the SK-N-AS (KRAS[Q61K] driven) NB cell line. As expected, the activation of ERK1/2 was unaffected by treatment with lorlatinib, since SK-N-AS is not an ALK-driven NB cell line. In contrast, the treatment of SK-N-AS with trametinib effectively blocked ERK1/2 phosphorylation and released the suppression of DLG2 expression in a time-dependent manner (Figures S6C and S6D). These data suggest that activation of the MEK/ERK signaling cascade, via ALK or other oncogenic drivers such as KRAS[Q61K], results in the suppression of DLG2 expression in NB cells.

SP1 Acts Downstream of ALK-ERK1/2 Signaling to Repress DLG2 Expression in NB

Having shown that ALK, acting through MAPK pathway signaling, transcriptionally regulates *DLG2* expression, we reasoned that this regulation may involve a transcriptional activator or a repressor downstream of ERK1/2. To identify potential TFs that may bind the *DLG2* promoter, we performed an *in silico* analysis of chromatin immunoprecipitation (ChIP)-seq data using the ChIPBase (http://rna.sysu.edu.cn/chipbase) online platform. This identified Specificity Protein 1 (SP1), which is known to be phosphorylated by ERK1/2, regulating its stability and DNA-binding properties (Beishline and Azizkhan-Clifford, 2015), as a potential candidate.

To investigate a role for SP1 in the regulation of *DLG2* expression, we treated two ALK-driven NB cell lines with increasing

concentrations of betulinic acid (BA), for 24 h. BA increases the sumoylation of SP1 protein by inhibiting SENP1 protease expression, leading to ubiquitin-mediated degradation of SP1 (Hsu et al., 2012). ALKi and MEKi were included as positive controls. BA treatment led to a decrease in SP1 protein levels as expected, together with a concomitant increase in DLG2 protein expression, with no effect on ERK1/2 phosphorylation (Figures 5A, 5B, S7A, and S7B). Treatment with either ALKi or MEKi resulted in the inhibition of ERK1/2 phosphorylation, decreased SP1 protein levels, and an increase in DLG2 expression, as expected. These data support a role for SP1 downstream of ERK1/2, which is consistent with previous reports (Beishline and Azizkhan-Clifford, 2015). We next used SP1-specific small interfering RNAs (siRNAs) to reduce SP1 protein levels in 3 independent NB cell lines. This resulted in an increase in DLG2 both at the mRNA and protein levels in all cases (Figures 5C–5G). To confirm a role for SP1 in the suppression of DLG2 expression downstream of ALK-ERK1/2, we generated an inducible SP1 NB cell line (SH-SY5Y-SP1[flag]). The induction of SP1 led to the repression of DLG2 expression (Figure S8A). Furthermore, SP1 expression blocked both lorlatinib- and trametinib-mediated upregulation of DLG2 (Figure S7C).

To determine whether SP1 directly binds to the *DLG2* promoter, we designed biotinylated DNA probes containing CHIP-predicted (http://rna.sysu.edu.cn/chipbase) SP1-binding sites containing regions of the *DLG2* locus (SP1-wt) (Figure 5H) and random sequence respectively (ctrl), in a DNA pull-down assay. SP1 was able to bind the SP1-wt probe but not the control probe (Figures 5I and 5J), while the non-biotinylated SP1-wt probe effectively competed SP1 binding (Figure 5K). We did not observe competition when the SP1-binding site was deleted (SP1-mut). These results suggest that SP1 acts as a transcriptional repressor downstream of the MAPK pathway to suppress *DLG2* expression in NB.

SP1 Knockdown Induces NB Differentiation through DLG2 Upregulation

Since SP1 represses the expression of *DLG2* and DLG2 overexpression leads to NB cell differentiation, we asked whether the loss of SP1 could also affect NB cell differentiation. In keeping with a role for SP1 in the regulation of *DLG2* expression, we also observed that siRNA-mediated knockdown of SP1 induced biochemical differentiation in SH-SY5Y, SK-N-SH, and SK-N-BE(2) NB cell lines as indicated by increased MAP2, NEFH, TrKA, and RET expression (Figures 6A, 6D, and 6G). Furthermore, SP1 knockdown significantly increased RA-mediated differentiation as compared to siRNA controls (siCtrl) (*p < 0.05, **p < 0.01, ***p < 0.001, ****p < 0.0001, Figures 6B, 6C, 6E, 6F, 6H, and 6I). In contrast, the overexpression of SP1 inhibited DLG2 expression and the downregulated expression of neuronal differentiation markers, and concomitantly inhibited RA-induced morphological differentiation (Figures S8A and S8B).

Since the loss of SP1 results in the upregulation of DLG2, we sought to determine whether DLG2 plays an important role in SP1-siRNA-induced differentiation. To do this, we transfected SH-SY5Y-shDLG2 cells with either SP1 siRNA (siSP1) or siCtrl before treatment with doxycycline or RA or both. The treatment of cells with doxycycline induced shRNA-mediated DLG2

knockdown, and resulted in the attenuation of siSP1-induced differentiation of NB cells both in the absence and presence of exogenous RA (Figure 6J). Specifically, SP1 knockdown spontaneously induced SH-SY5Y-shDLG2 cell differentiation in the absence of RA, and this was significantly inhibited upon doxycycline-induced DLG2 knockdown (Figure 6J). Our data show that SP1 negatively regulates *DLG2* and that SP1 knockdown enhances NB differentiation. From the Asgharzadeh patient cohort (https://hgserver1.amc.nl:443/), we found an inverse correlation between *SP1* and *DLG2* expression (data not shown). In this cohort, tumors are histologically graded, allowing the examination of SP1/DLG2 with respect to tumor differentiation status. *DLG2* was more highly expressed in differentiated tumors, in contrast to *SP1*, which exhibited expression in tumors with undifferentiated or poorly differentiated histology (Figures 6K and 6L). These findings suggest a potential clinical relevance of *DLG2* and *SP1* as biomarkers for NB tumor prognosis.

Analysis of 11q del Tumors Identifies *DLG2* Aberrations in NB

NB tumor samples (n = 436) were screened by SNP array to investigate copy-number variants and allelic imbalances on 11q. Deletions involving 11q were identified in 218 of 436 tumors (detailed in Table S2). Of these, 2 types of chromosome 11 aberrations were observed. The first was a relative loss of the entire chromosome 11 (98/218 tumors, 45%); these tumors predominantly showed an overall pattern of numerical imbalances. The second was segmental loss—in other words, partial 11q loss (120/218 tumors, 55%) (Table S2). No homozygous 11q losses were observed. Of the 120 tumors with partial 11q del, all except 10 cases had deletions extending from the breakpoint to the q-terminal of chromosome 11 (Figure 7A).

Chromosome 11q loss and amplification of *MYCN* constitute the 2 major NB unfavorable prognosis groups. In general, there is an inverse correlation between 11q loss and MYCN amplification (Carén et al., 2010; Chen et al., 2004; Guo et al., 1999). However, in a small group of NB cases, both of these features occur simultaneously. In the series of 120 NB tumors with segmental chromosome 11 deletion, we noted that 26 cases had both MYCN amplification (MNA) and 11q del, while the remaining 94 had 11q del to varying degrees, in the absence of MNA (Figure 7A; Table S2). In analyzing the chromosome aberration patterns of these 2 NB groups, we noted that cases with 11q del and *MYCN* amplification (here denoted 11q del + MNA) and those with 11q del without *MYCN* amplification (here called 11q del) exhibit different 11q del patterns (Figure 7B). Examination of the SRO (shortest region of overlap of deletions) showed that the 11q del + MNA subgroup in general displays more distal 11q del breakpoints (SRO ranging from Chr11:105 to 115 Mb (hg19) from pter), while the 11q del group that lacks MNA has a more proximal 11q breakpoint pattern (Figures 7A and 7B) (SRO chr11:85–103 Mb). There are 84 putative candidate genes in the proximal SRO (chr11:85–103) (hg19) in 11q del NB from our patient group (Table S3). *DLG2* is the most proximal of the 84 genes, harboring a cluster of breakpoints that potentially disrupt the *DLG2* locus (Figures 7B, S9A, and S9B). A total of 17 of120 clustered from both the 11q del and the 11q del + MNA subgroup, which display proximal deletion breakpoints either in or
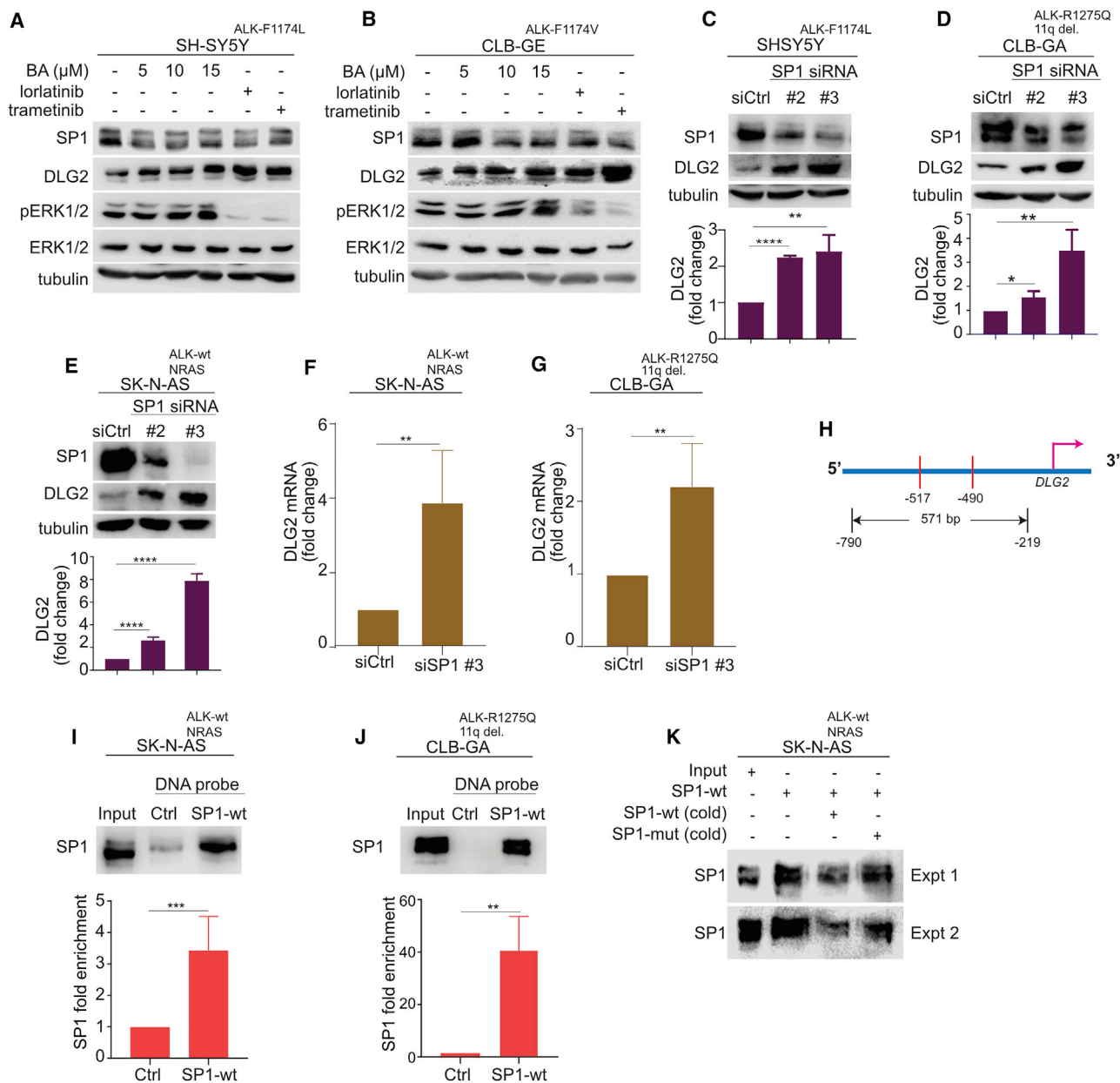
Figure 5. SP1 Acts Downstream of the ALK-ERK1/2 Signaling Axis to Repress *DLG2* Expression in NB

(A and B) Western blot analyses of SP1, DLG2, and indicated proteins in whole-cell lysates of SH-SY5Y and CLB-GE NB cell lines treated with betulinic acid (BA), at increasing concentrations for 24 h.
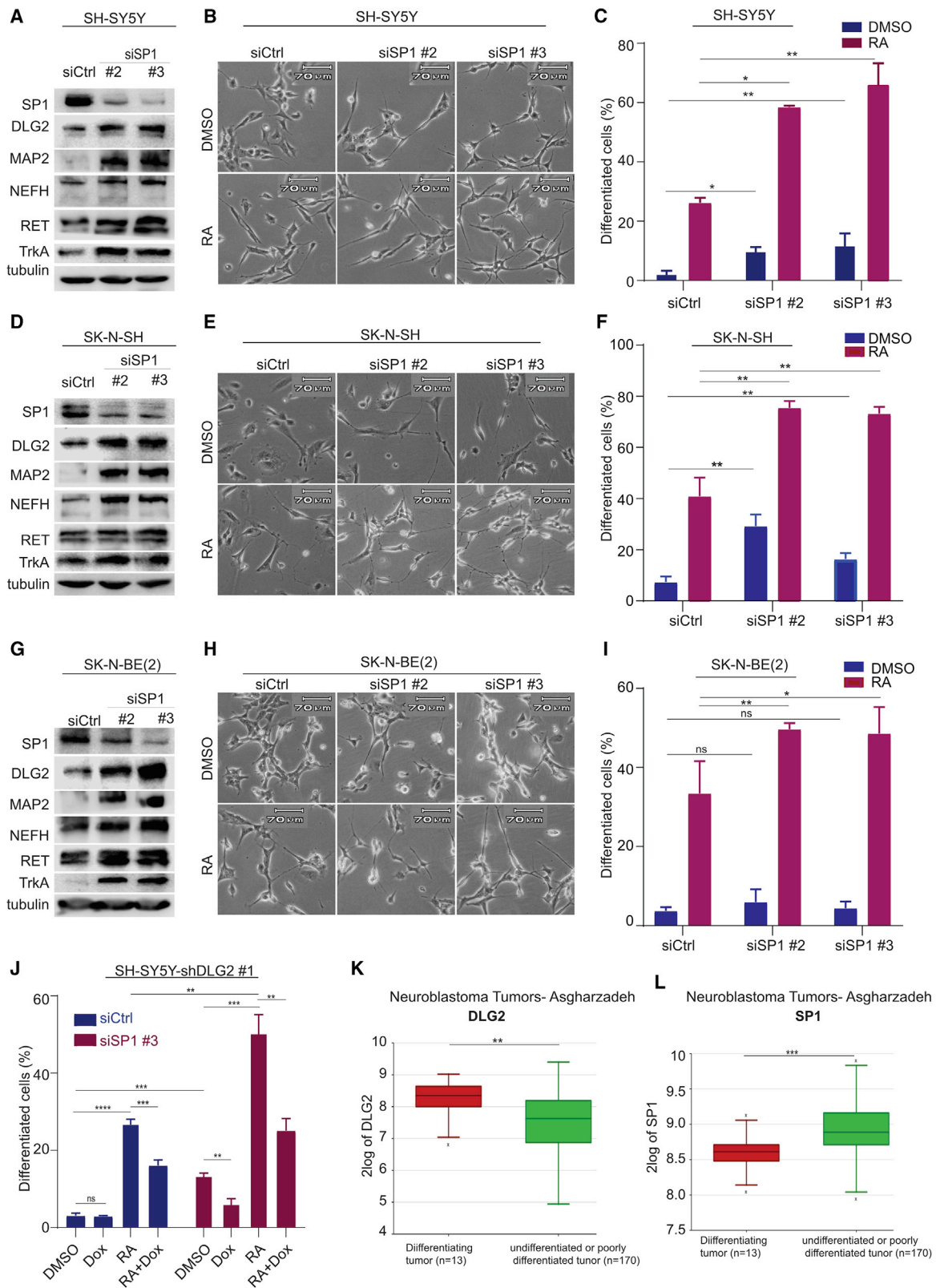
(C–E) Western blot analysis of the effect of SP1 siRNA on DLG2 expression levels. SH-SY5Y (C), CLB-GA (D), and SK-N-AS (E) were transfected with either scrambled control (siCtrl) or 2 independent siRNAs targeting SP1. Whole-cell lysates were western blotted for SP1, DLG2, and tubulin as loading control.

(F and G) qPCR analysis of *DLG2* mRNA levels in SK-N-AS (F) and CLB-GA (G) transfected with either scrambled control (siCtrl) or siRNA targeting SP1.

(H) Schematic depicting the *DLG2* promoter region. Red bars indicate the predicted SP1-binding motifs and the 571 bp between black bars indicate the predicted SP1-binding region used as probe.

(I and J) Nuclear extracts from either SK-N-AS (I) or CLB-GA (J) were incubated for 90 min with biotinylated DNA probes (ctrl versus SP1-wt), and SP1-binding enrichment was analyzed by western blot, quantified below.

(K) Western blot analysis of the competitive effect of either SP1 (SP1-wt) or SP1 mutant (SP1-mut) non-biotinylated (cold) DNA probes on SP1 protein binding to the *DLG2* promotor probe. Competitor cold DNA probes (15 μg) were incubated with nuclear extract 90 min before the addition of the biotinylated SP1-wt probe. Unpaired t test. *$p < 0.05$, **$p < 0.01$, and ****$p < 0.0001$. Quantified data are means ± SDs of at least 3 independent experiments.

A SH-SY5Y

B SH-SY5Y

C SH-SY5Y

D SK-N-SH

E SK-N-SH

F SK-N-SH

G SK-N-BE(2)

H SK-N-BE(2)

I SK-N-BE(2)

J SH-SY5Y-shDLG2 #1

K Neuroblastoma Tumors- Asgharzadeh
DLG2

L Neuroblastoma Tumors- Asgharzadeh
SP1

(legend on next page)

in close proximity to the *DLG2* gene. Furthermore, within the 11q del, 12 tumors were found with disrupting tumor-specific rearrangements either in or in close proximity to the *DLG2* gene (Figures 7C, S9A, and S9B). Analysis of the expression levels of the 84 candidates in NB tumor material identified 15 genes, including *DLG2*, that exhibited a lower expression level in unfavorable NB with significant p values (https://hgserver1.amc.nl:443/; 1.0e−3 to 9.8e−8, Versteeg-88 cohort; Table S3). Therefore, *DLG2* is a strong candidate NB tumor suppressor gene in the high-risk non-*MYCN* amplified NB tumors with 11q del, based on position, high number of breakpoints, and expression levels in tumors (Figures 7, S9A, and S9B; Table S3). This is in agreement with our earlier observations (Figures 1B, 6K, and S1), showing that high *DLG2* mRNA expression levels correlate with better patient prognosis. Moreover, overall survival analysis of NB patient data from this cohort of 436 NB tumor cases suggests that patients with 11q del NB have a poor prognosis, similar to the MNA category (Figure 7D). We also observed that patients with 11q del + MNA, although rare, exhibit the worst prognostic outcomes (Figure 7D). Thus, our genetic data support the disruption of the *DLG2* gene as a tumor suppressor gene target of the 11q loss of heterozygosity (LOH) observed in NB.

DISCUSSION

Our present understanding of NB tumorigenesis suggests that 11q loss is acquired in unfavorable late-presenting NB (Carén et al., 2010). This analysis of a 436-strong NB patient cohort supports the poor prognosis of 11q del NB patients, which is comparable with the high-risk MYCN-amplified patient group. We also note that patients harboring both 11q del and MYCN amplification, although rare, constitute an ultra-high-risk group of NB patients. Our genomic and experimental analysis supports *DLG2* as a potential tumor suppressor gene mapping within the critical 11q del region that is rearranged or deleted in a subset of high-risk NB. The 11q chromosomal rearrangements identified here potentially interfere with *DLG2* function by directly disrupting the normal gene structure or upstream regulatory regions. The Knudson model for LOH involving tumor suppressor genes suggests that the remaining *DLG2* allele in these NB tumors may harbor deleterious mutations. However, we did not find any genetic lesions in the remaining *DLG2* allele in our cohort, suggesting that gene-dosage mechanisms are involved. Haploinsufficiency has been shown to contribute to tumor development in a number of examples, such as p27, Hint1, and Dmp1, where the remaining intact wild-type allele is insufficient to suppress tumor

growth (Fero et al., 1998; Inoue et al., 2001; Li et al., 2006). It may also be the case that losses of additional genetic loci on 11q contribute in the complex genetic landscape of patient tumors. For example, many genes coding for proteins in the DNA damage response (e.g., *ATM*, *CHEK1*, *H2AFX*, and *MRE11*) are located on 11q, in addition to *PHOX2A*, *CCND1*, *SDHD*, and *CADM1*, which have been investigated as 11q candidate loci (Mlakar et al., 2017).

This work establishes an important function of DLG2 in NB cell differentiation that is consistent with a tumor suppressor function, and identifies underlying molecular mechanisms by which ALK-ERK1/2 activity suppresses *DLG2* expression. These findings are in keeping with single-cell expression data of the developing murine neural crest, in which *DLG2* was noted to be one of the transition bridge cell genes that are expressed during the differentiation of precursor cells destined to become sympathetic neurons or chromaffin cells of the adrenal medulla (Furlan et al., 2017). By examining the bridge cell genes in the context of NB patient tumor material, we show that high expression of late peak time bridge cell genes (i.e., those upregulated over time in this cell population) strongly correlates with better prognosis. In contrast, high expression of early peak time bridge cell genes (i.e., those downregulated over time in this cell population) correlates with poor prognosis. These findings suggest an important role for the bridge cell genes in differentiation and suggest that their perturbation likely promotes NB progression.

Although *Dlg* has been shown to be a tumor suppressor in *Drosophila* and its human homolog *DLG2* has also recently been implicated in osteosarcoma tumorigenesis (Shao et al., 2019; Woods and Bryant, 1991), a role for DLG2 in NB has not been investigated. Our initial experiments overexpressing DLG2 resulted in the inhibition of growth of NB cells *in vitro*, an effect that was confirmed in mouse xenografts, in which DLG2 expression robustly reduced tumor burden. The overexpression of DLG2 also promoted neuronal differentiation to levels similar to those previously reported for RA-induced differentiation (Kasim et al., 2016; Pandey et al., 2014). To our knowledge RA-induced differentiation results in an incomplete response in NB cells, with up to 30% of cells differentiating. Moreover, the underlying mechanism of differentiation is unclear. One explanation for these observations was suggested recently by van Groningen and colleagues (van Groningen et al., 2017), who showed that NB is composed of two cell types: MES and ADRN cells. Their work highlighted the high level of transcriptional plasticity exhibited by NB cells, which is reflected in the ability of MES or

Figure 6. SP1 Knockdown Induces NB Differentiation
(A, D, and G) Western blot analyses of differentiation markers in SH-SY5Y (A), SK-N-SH (D), and SK-N-BE(2) (G) NB cells, transfected with either scrambled control (siCtrl) or 2 independent siRNAs targeting SP1.
(B, E, and H) Representative images of neurite outgrowth in SH-SY5Y (B), SK-N-SH (E), and SK-N-BE(2) (H).
(C, F, and I) Quantification of neurite outgrowth in SH-SY5Y (C), SK-N-SH (F), and SK-N-BE(2) (I).
(J) The SH-SY5Y-shDLG2 cell line stably expresses an inducible *DLG2* shRNA. Cells were transfected with either siCtrl or siRNA targeting SP1 (siSP1), as indicated. The bar graph shows the effect of Dox-induced *DLG2* knockdown on *SP1* siRNA-mediated differentiation in SH-SY5Y-shDLG2 cells.
(K and L) Boxplots showing the correlation between tumor grade (differentiated or undifferentiated) and DLG2 (K) or SP1 (L) mRNA expression in NB tumor samples.
Unpaired t test. *p < 0.05, **p < 0.01, ***p < 0.001, and ****p < 0.0001; ns, not significant. Quantified data are means ± SDs of at least 3 independent experiments. Scale bar (B, E, and H) 70 μM.
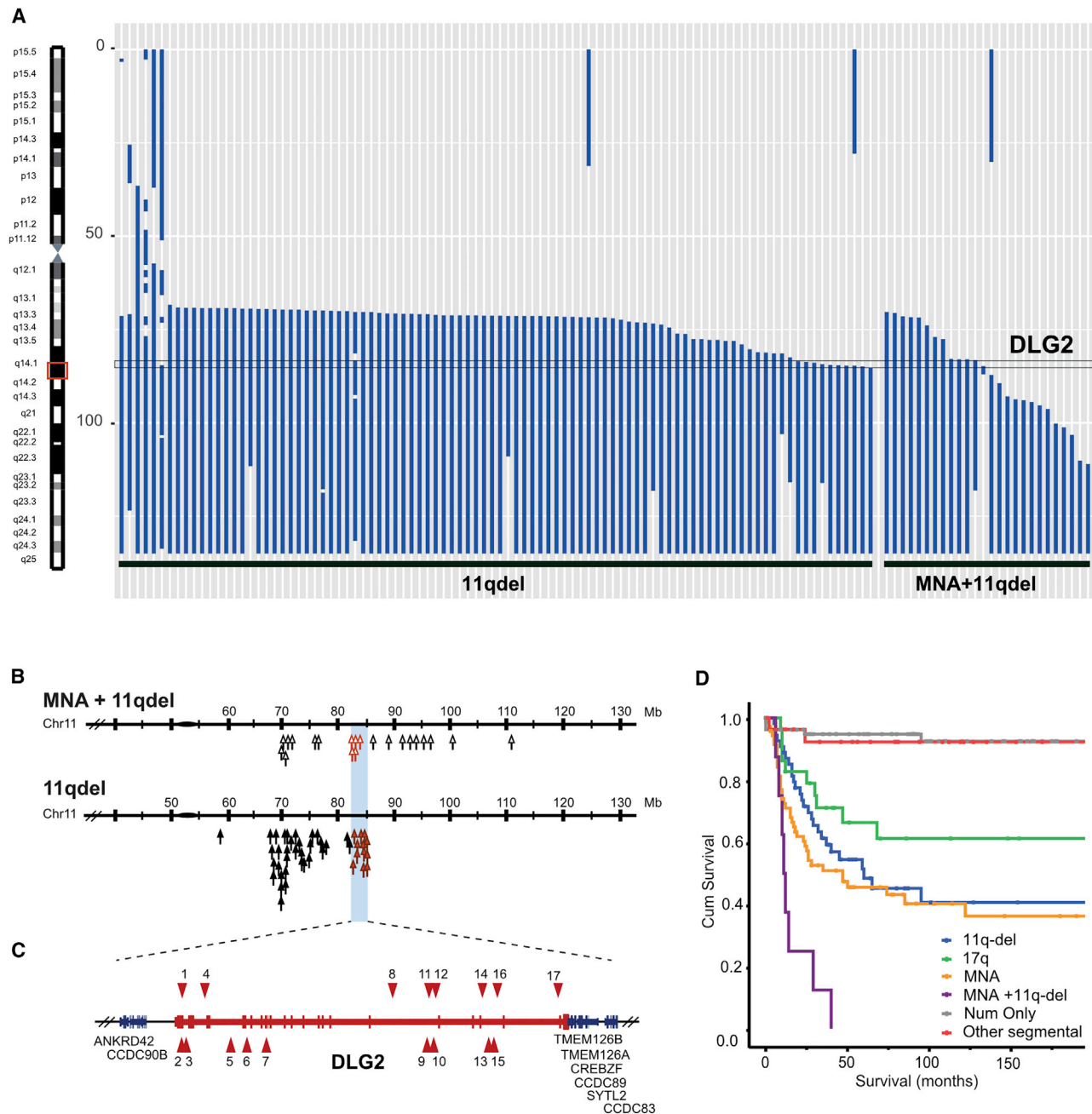
Figure 7. Genetic Analysis of 11q Deletions (11q del) in NB Patients Identifies Breakpoints in *DLG2*
(A) Summary of SNP array genomic profiles showing deletions on chromosome 11q. The genomic position of the *DLG2* locus on chromosome 11 is indicated at left (red box). Each vertical line represents 1 NB tumor and the deleted region is indicated (scale to the left in megabase distances from pter [the short arm telomere]). Cases with 11q del and *MYCN* amplification are denoted MNA[+]11q; those with 11q del without *MYCN* amplification are denoted 11q del.
(B and C) Cluster of breakpoints and aberrations on 11q. SNP array data breakpoints in MNA[+]11q cases (B) and 11q del cases (without MNA) (C).
(D) Kaplan-Maier overall survival analysis of the patient data. Patient data are based on the genomic profiles of 436 NB tumor cases (see Table S2).

ADRN cells to transdifferentiate to either cell type. Furthermore, MES cells are resistant to therapy and RA-induced differentiation *in vitro* (Arumugam et al., 2009; Naiditch et al., 2015; Piskareva et al., 2015). In our analyses, we also observe an incomplete differentiation response to RA alone. However, the treatment of

DLG2-overexpressing NB cells with either RA or NGF results in a striking synergistic effect, with 90%–100% of cells undergoing differentiation. This clearly indicates a role for DLG2 as an integral component of the differentiation process. The importance of DLG2 is further highlighted by the finding that RA treatment

itself upregulates *DLG2* expression, and that loss of DLG2 inhibits RA-induced differentiation in NB cells.

An additional intriguing observation arose from our RNA-seq analyses of NB cells expressing DLG2 in comparison with those treated with RA. Analyzing these data based on the reported MES and ADRN signatures (van Groningen et al., 2017) revealed a clear difference in the "differentiation" responses at the mRNA level, with *DLG2* expression strongly promoting an ADRN signature, whereas RA treatment promoted a mixed ADRN/MES signature. NB cells that exhibit a more stringent ADRN identity, such as DLG2-expressing cells, may represent a more completely differentiated state, in keeping with the observation that DLG2 expression appears in the later stages of the reconstructed differentiation time course of the SCP-chromaffin path (Furlan et al., 2017). This is in keeping with DLG2's increasing the ADRN score of NB cells and potentiating RA-induced neuritogenesis. The molecular mechanisms underlying the ability of DLG2 to regulate transcription during differentiation are unknown at present, although our RNA-seq results do identify some interesting differences in comparison with RA-induced differentiation. Analysis of RA-induced differentiation identified a clear RA receptor (RARA/B) signature, which was not observed in DLG-induced differentiation. Conversely, DLG-induced differentiation appears to involve the modulation of genes by TFs such as REST, SMAD1, TBP, and TCF4. How DLG2 modulates these transcriptional changes is unclear, and is an interesting topic for future investigation.

One implication of these findings is that therapeutic approaches that result in an increased ADRN score and/or decrease the MES score of NB tumors could enhance RA-induced differentiation, which may increase the modest clinical efficacy of RA therapy. One such preclinical approach is the silencing of the SP1 transcriptional repressor, which we show here leads to an increase in DLG2 expression and the induction of neuritogenesis, and further potentiates the RA-induced differentiation of NB cells. It is known that the expression of the human ALK^{F1174L}-activated mutant in mouse neural crest cells significantly impairs early sympathetic progenitor differentiation and increases their proliferation (Vivancos Stalin et al., 2019). In addition, we have previously shown that the treatment of an ALK$^+$ NB patient with ALKi significantly reduced the primary tumor size and the resected tumor demonstrated significant differentiation, resembling ganglioneuroblastoma (Guan et al., 2018). The identification of DLG2 as a key differentiation component that is repressed by oncogenic ALK-ERK1/2 signaling provides a mechanistic link between ALK-driven NB and the inhibition of the differentiation process. Intuitively, one would suggest combining MEKi and RA to synergistically promote differentiation; however, MAPK/ERK1/2 is also important in both RA- and NGF-mediated neuronal differentiation, thereby making the identification and the precise targeting of the anti-differentiation signaling axis downstream of ERK1/2 essential. Furthermore, ALK-dependent NB appears to be less sensitive to MEK inhibition due to feedback mechanisms that increase the activity of other proliferation and survival pathways (Umapathy et al., 2017). While we show here that SP1 acts downstream of ALK-ERK1/2 signaling axis to block NB differentiation through the repression of DLG2 expression, further investigation will be required to clarify therapeutic approaches that will be of benefit to NB patients.

In summary, our data suggest that an important role for oncogenic ALK-ERK1/2-SP1 signaling is the maintenance of an undifferentiated state of transformed NC-derived progenitors through *DLG2* repression. The importance of SP1 and DLG2 in this process is highlighted by the findings that restoring DLG2 expression (e.g., by expressing DLG2 or targeting SP1) potently drives NB differentiation. Furthermore, we show in a clinical cohort of 436 patient tumors that the *DLG2* gene genetically maps to a region on 11q that has a high frequency of aberrations in NB. Our analysis of *DLG2* also suggests that further exploration of other bridge cell genes may help us to understand the mechanisms underlying the differentiation of SCPs and SA cells and their contribution to NB. In this work, we uncover a role for ALK and other oncogenes driving ERK signaling in NB tumorigenesis. ALK not only promotes the proliferation and survival of NB cells but it also suppresses their differentiation by negatively regulating the expression of *DLG2*, which is frequently deleted in high-risk NB. The remaining intact *DLG2* allele in 11q del NB is transcriptionally responsive to ALK and ERK pathway inhibition, leading to increased expression of the DLG2 tumor suppressor protein. Thus, a subset of 11q del NB may be responsive to ALK and MEK TKI treatment as a therapeutic option.

STAR★METHODS

Detailed methods are provided in the online version of this paper and include the following:

- KEY RESOURCES TABLE
- RESOURCE AVAILABILITY
  - Lead contact
  - Materials Availability
  - Data and Code Availability
- EXPERIMENTAL MODEL AND SUBJECT DETAILS
  - Cell culture, cell lysis and western blot
  - Human patients
  - Mouse models/animals
- METHOD DETAILS
  - Immunoblotting
  - Plasmid cloning and lentivirus
  - Cell proliferation, cell cycle and differentiation assays
  - RNA extraction and Quantitative PCR
  - Nuclear extract isolation and DNA probe pulldown assay
  - Mouse xenografts
  - RNA-Seq data analysis
  - Proteomic Tandem Mass Tag labeling and LC-MS/MS analysis
  - SNP microarray analysis and whole genome sequencing
- QUANTIFICATION AND STATISTICAL ANALYSIS

Cell Reports
Article

AUTHOR CONTRIBUTIONS

J.T.S., R.H.P., and B.H. conceived and designed the cell biology experiments. J.T.S. conducted all of the wet lab experimental analyses in the study, excluding the xenograft experiments, which were performed by D.E.L. and W.-Y.L. J.V.d.E. analyzed all of the other RNA-seq and proteomic datasets and performed the bioinformatics analyses. T.M. and N.J. conceived and designed the genetic and bioinformatics analyses of NB tumors, together with S.F., A.D., R.-M.S., A.M.-M., M.Ö., H.C., G.T., K.B., A.P.B., and R.N. R.N., K.B., and P.K. collected the tumor material and corresponding clinical information. J.T.S., R.H.P., and B.H. wrote the manuscript, with input from all of the other authors. All of the authors discussed results from the experiments and commented on the manuscript.

DECLARATION OF INTERESTS

The authors declare no competing interests.

REFERENCES

Anders, S., Pyl, P.T., and Huber, W. (2015). HTSeq–a Python framework to work with high-throughput sequencing data. Bioinformatics 31, 166–169.

Arumugam, T., Ramachandran, V., Fournier, K.F., Wang, H., Marquis, L., Abbruzzese, J.L., Gallick, G.E., Logsdon, C.D., McConkey, D.J., and Choi, W. (2009). Epithelial to mesenchymal transition contributes to drug resistance in pancreatic cancer. Cancer Res. 69, 5820–5828.

Beishline, K., and Azizkhan-Clifford, J. (2015). Sp1 and the 'hallmarks of cancer'. FEBS J. 282, 224–258.

Benjamini, Y., and Hochberg, Y. (1995). Controlling the False Discovery Rate - a Practical and Powerful Approach to Multiple Testing. J. R. Stat. Soc. Series B Stat. Methodol. 57, 289–300.

Brodeur, G.M. (2003). Neuroblastoma: biological insights into a clinical enigma. Nat. Rev. Cancer 3, 203–216.

Brodeur, G.M., and Bagatell, R. (2014). Mechanisms of neuroblastoma regression. Nat. Rev. Clin. Oncol. 11, 704–713.

Carén, H., Abel, F., Kogner, P., and Martinsson, T. (2008). High incidence of DNA mutations and gene amplifications of the ALK gene in advanced sporadic neuroblastoma tumours. Biochem. J. 416, 153–159.

Carén, H., Kryh, H., Nethander, M., Sjöberg, R.M., Träger, C., Nilsson, S., Abrahamsson, J., Kogner, P., and Martinsson, T. (2010). High-risk neuroblastoma tumors with 11q-deletion display a poor prognostic, chromosome instability phenotype with later onset. Proc. Natl. Acad. Sci. USA 107, 4323–4328.

Chand, D., Yamazaki, Y., Ruuth, K., Schönherr, C., Martinsson, T., Kogner, P., Attiyeh, E.F., Maris, J., Morozova, O., Marra, M.A., et al. (2013). Cell culture and

Drosophila model systems define three classes of anaplastic lymphoma kinase mutations in neuroblastoma. Dis. Model. Mech. 6, 373–382.

Chang, H.H., Lu, M.Y., Yang, Y.L., Chou, S.W., Lin, D.T., Lin, K.H., Hsu, W.M., Jeng, Y.M., and Jou, S.T. (2020). The prognostic roles of and correlation between ALK and MYCN protein expression in neuroblastoma. J. Clin. Pathol. 73, 154–161.

Chen, Q.R., Bilke, S., Wei, J.S., Whiteford, C.C., Cenacchi, N., Krasnoselsky, A.L., Greer, B.T., Son, C.G., Westermann, F., Berthold, F., et al. (2004). cDNA array-CGH profiling identifies genomic alterations specific to stage and MYCN-amplification in neuroblastoma. BMC Genomics 5, 70.

Chen, X., Schulz-Trieglaff, O., Shaw, R., Barnes, B., Schlesinger, F., Källberg, M., Cox, A.J., Kruglyak, S., and Saunders, C.T. (2016). Manta: rapid detection of structural variants and indels for germline and cancer sequencing applications. Bioinformatics 32, 1220–1222.

Cheung, Y.T., Lau, W.K., Yu, M.S., Lai, C.S., Yeung, S.C., So, K.F., and Chang, R.C. (2009). Effects of all-trans-retinoic acid on human SH-SY5Y neuroblastoma as in vitro model in neurotoxicity research. Neurotoxicology 30, 127–135.

Chu, P.W., Cheung, W.M., and Kwong, Y.L. (2003). Differential effects of 9-cis, 13-cis and all-trans retinoic acids on the neuronal differentiation of human neuroblastoma cells. Neuroreport 14, 1935–1939.

Cole, K.A., Huggins, J., Laquaglia, M., Hulderman, C.E., Russell, M.R., Bosse, K., Diskin, S.J., Attiyeh, E.F., Sennett, R., Norris, G., et al. (2011). RNAi screen of the protein kinome identifies checkpoint kinase 1 (CHK1) as a therapeutic target in neuroblastoma. Proc. Natl. Acad. Sci. USA 108, 3336–3341.

De Brouwer, S., De Preter, K., Kumps, C., Zabrocki, P., Porcu, M., Westerhout, E.M., Lakeman, A., Vandesompele, J., Hoebeeck, J., Van Maerken, T., et al. (2010). Meta-analysis of neuroblastomas reveals a skewed ALK mutation spectrum in tumors with MYCN amplification. Clin. Cancer Res. 16, 4353–4362.

de Thé, H. (2018). Differentiation therapy revisited. Nat. Rev. Cancer 18, 117–127.

Emdal, K.B., Pedersen, A.K., Bekker-Jensen, D.B., Tsafou, K.P., Horn, H., Lindner, S., Schulte, J.H., Eggert, A., Jensen, L.J., Francavilla, C., and Olsen, J.V. (2015). Temporal proteomics of NGF-TrkA signaling identifies an inhibitory role for the E3 ligase Cbl-b in neuroblastoma cell differentiation. Sci. Signal. 8, ra40.

Fero, M.L., Randel, E., Gurley, K.E., Roberts, J.M., and Kemp, C.J. (1998). The murine gene p27Kip1 is haplo-insufficient for tumour suppression. Nature 396, 177–180.

Fieuw, A., De Wilde, B., Speleman, F., Vandesompele, J., and De Preter, K. (2012). Cancer gene prioritization for targeted resequencing using FitSNP scores. PLOS ONE 7, e31333.

Furlan, A., Dyachuk, V., Kastriti, M.E., Calvo-Enrique, L., Abdo, H., Hadjab, S., Chontorotzea, T., Akkuratova, N., Usoskin, D., Kamenev, D., et al. (2017). Multipotent peripheral glial cells generate neuroendocrine cells of the adrenal medulla. Science 357, eaal3753.

Gröbner, S.N., Worst, B.C., Weischenfeldt, J., Buchhalter, I., Kleinheinz, K., Rudneva, V.A., Johann, P.D., Balasubramanian, G.P., Segura-Wang, M., Brabetz, S., et al.; ICGC PedBrain-Seq Project; ICGC MMML-Seq Project (2018). The landscape of genomic alterations across childhood cancers. Nature 555, 321–327.

Guan, J., Fransson, S., Siaw, J.T.T., Treis, D., Van den Eynden, J., Chand, D., Umapathy, G., Ruuth, K., Svenberg, P., Wessman, S., et al. (2018). Clinical response of the novel activating ALK-I1171T mutation in neuroblastoma to the ALK inhibitor ceritinib. Cold Spring Harb. Mol. Case Stud. 4, a002550.

Guo, C., White, P.S., Weiss, M.J., Hogarty, M.D., Thompson, P.M., Stram, D.O., Gerbing, R., Matthay, K.K., Seeger, R.C., Brodeur, G.M., and Maris, J.M. (1999). Allelic deletion at 11q23 is common in MYCN single copy neuroblastomas. Oncogene 18, 4948–4957.

Harrow, J., Frankish, A., Gonzalez, J.M., Tapanari, E., Diekhans, M., Kokocinski, F., Aken, B.L., Barrell, D., Zadissa, A., Searle, S., et al. (2012). GENCODE: the reference human genome annotation for The ENCODE Project. Genome Res. 22, 1760–1774.

He, W.G., Yan, Y., Tang, W., Cai, R., and Ren, G. (2017). Clinical and biological features of neuroblastic tumors: A comparison of neuroblastoma and ganglioneuroblastoma. Oncotarget 8, 37730–37739.

Hoehner, J.C., Olsen, L., Sandstedt, B., Kaplan, D.R., and Påhlman, S. (1995). Association of neurotrophin receptor expression and differentiation in human neuroblastoma. Am. J. Pathol. 147, 102–113.

Hoehner, J.C., Gestblom, C., Hedborg, F., Sandstedt, B., Olsen, L., and Påhlman, S. (1996). A developmental model of neuroblastoma: differentiating stroma-poor tumors' progress along an extra-adrenal chromaffin lineage. Lab. Invest. 75, 659–675.

Hsu, T.I., Wang, M.C., Chen, S.Y., Yeh, Y.M., Su, W.C., Chang, W.C., and Hung, J.J. (2012). Sp1 expression regulates lung tumor progression. Oncogene 31, 3973–3988.

Huber, K., Kalcheim, C., and Unsicker, K. (2009). The development of the chromaffin cell lineage from the neural crest. Auton. Neurosci. 151, 10–16.

Inoue, K., Zindy, F., Randle, D.H., Rehg, J.E., and Sherr, C.J. (2001). Dmp1 is haplo-insufficient for tumor suppression and modifies the frequencies of Arf and p53 mutations in Myc-induced lymphomas. Genes Dev. 15, 2934–2939.

Kasim, M., Heß, V., Scholz, H., Persson, P.B., and Fähling, M. (2016). Achaete-Scute Homolog 1 Expression Controls Cellular Differentiation of Neuroblastoma. Front. Mol. Neurosci. 9, 156.

Kim, D., Langmead, B., and Salzberg, S.L. (2015). HISAT: a fast spliced aligner with low memory requirements. Nat. Methods 12, 357–360.

Li, H., Zhang, Y., Su, T., Santella, R.M., and Weinstein, I.B. (2006). Hint1 is a haplo-insufficient tumor suppressor in mice. Oncogene 25, 713–721.

Liu, Z.-P., Wu, C., Miao, H., and Wu, H. (2015). RegNetwork: an integrated database of transcriptional and post-transcriptional regulatory networks in human and mouse. Database 2015 (bav095). https://doi.org/10.1093/database/bav095. https://academic.oup.com/database/article/doi/10.1093/database/bav095/2433227.

Love, M.I., Huber, W., and Anders, S. (2014). Moderated estimation of fold change and dispersion for RNA-seq data with DESeq2. Genome Biol. 15, 550.

Lucarelli, E., Kaplan, D.R., and Thiele, C.J. (1995). Selective regulation of TrkA and TrkB receptors by retinoic acid and interferon-gamma in human neuroblastoma cell lines. J. Biol. Chem. 270, 24725–24731.

Maris, J.M. (2010). Recent advances in neuroblastoma. N. Engl. J. Med. 362, 2202–2211.

Maris, J.M., Guo, C., White, P.S., Hogarty, M.D., Thompson, P.M., Stram, D.O., Gerbing, R., Matthay, K.K., Seeger, R.C., and Brodeur, G.M. (2001). Allelic deletion at chromosome bands 11q14-23 is common in neuroblastoma. Med. Pediatr. Oncol. 36, 24–27.

Maris, J.M., Hogarty, M.D., Bagatell, R., and Cohn, S.L. (2007). Neuroblastoma. Lancet 369, 2106–2120.

Marshall, C.R., Noor, A., Vincent, J.B., Lionel, A.C., Feuk, L., Skaug, J., Shago, M., Moessner, R., Pinto, D., Ren, Y., et al. (2008). Structural variation of chromosomes in autism spectrum disorder. Am. J. Hum. Genet. 82, 477–488.

Masetti, R., Biagi, C., Zama, D., Vendemini, F., Martoni, A., Morello, W., Gasperini, P., and Pession, A. (2012). Retinoids in pediatric onco-hematology: the model of acute promyelocytic leukemia and neuroblastoma. Adv. Ther. 29, 747–762.

Matthay, K.K., Villablanca, J.G., Seeger, R.C., Stram, D.O., Harris, R.E., Ramsay, N.K., Swift, P., Shimada, H., Black, C.T., Brodeur, G.M., et al.; Children's Cancer Group (1999). Treatment of high-risk neuroblastoma with intensive chemotherapy, radiotherapy, autologous bone marrow transplantation, and 13-cis-retinoic acid. N. Engl. J. Med. 341, 1165–1173.

Matthay, K.K., Reynolds, C.P., Seeger, R.C., Shimada, H., Adkins, E.S., Haas-Kogan, D., Gerbing, R.B., London, W.B., and Villablanca, J.G. (2009). Long-term results for children with high-risk neuroblastoma treated on a randomized trial of myeloablative therapy followed by 13-cis-retinoic acid: a children's oncology group study. J. Clin. Oncol. 27, 1007–1013.

Mlakar, V., Jurkovic Mlakar, S., Lopez, G., Maris, J.M., Ansari, M., and Gumy-Pause, F. (2017). 11q deletion in neuroblastoma: a review of biological and clinical implications. Mol. Cancer 16, 114.

Murillo, J.R., Goto-Silva, L., Sánchez, A., Nogueira, F.C.S., Domont, G.B., and Junqueira, M. (2017). Quantitative proteomic analysis identifies proteins and pathways related to neuronal development in differentiated SH-SY5Y neuroblastoma cells. EuPA Open Proteom. 16, 1–11.

Naiditch, J.A., Jie, C., Lautz, T.B., Yu, S., Clark, S., Voronov, D., Chu, F., and Madonna, M.B. (2015). Mesenchymal change and drug resistance in neuroblastoma. J. Surg. Res. 193, 279–288.

Nannya, Y., Sanada, M., Nakazaki, K., Hosoya, N., Wang, L., Hangaishi, A., Kurokawa, M., Chiba, S., Bailey, D.K., Kennedy, G.C., and Ogawa, S. (2005). A robust algorithm for copy number detection using high-density oligonucleotide single nucleotide polymorphism genotyping arrays. Cancer Res. 65, 6071–6079.

Pandey, G.K., Mitra, S., Subhash, S., Hertwig, F., Kanduri, M., Mishra, K., Fransson, S., Ganeshram, A., Mondal, T., Bandaru, S., et al. (2014). The risk-associated long noncoding RNA NBAT-1 controls neuroblastoma progression by regulating cell proliferation and neuronal differentiation. Cancer Cell 26, 722–737.

Park, J.R., Bagatell, R., London, W.B., Maris, J.M., Cohn, S.L., Mattay, K.K., and Hogarty, M.; COG Neuroblastoma Committee (2013). Children's Oncology Group's 2013 blueprint for research: neuroblastoma. Pediatr. Blood Cancer 60, 985–993.

Piskareva, O., Harvey, H., Nolan, J., Conlon, R., Alcock, L., Buckley, P., Dowling, P., Henry, M., O'Sullivan, F., Bray, I., and Stallings, R.L. (2015). The development of cisplatin resistance in neuroblastoma is accompanied by epithelial to mesenchymal transition in vitro. Cancer Lett. 364, 142–155.

Pugh, T.J., Morozova, O., Attiyeh, E.F., Asgharzadeh, S., Wei, J.S., Auclair, D., Carter, S.L., Cibulskis, K., Hanna, M., Kiezun, A., et al. (2013). The genetic landscape of high-risk neuroblastoma. Nat. Genet. 45, 279–284.

Roberts, S., Delury, C., and Marsh, E. (2012). The PDZ protein discs-large (DLG): the 'Jekyll and Hyde' of the epithelial polarity proteins. FEBS J. 279, 3549–3558.

Roller, E., Ivakhno, S., Lee, S., Royce, T., and Tanner, S. (2016). Canvas: versatile and scalable detection of copy number variants. Bioinformatics 32, 2375–2377.

Russo, V.C., Schütt, B.S., Andaloro, E., Ymer, S.I., Hoeflich, A., Ranke, M.B., Bach, L.A., and Werther, G.A. (2005). Insulin-like growth factor binding protein-2 binding to extracellular matrix plays a critical role in neuroblastoma cell proliferation, migration, and invasion. Endocrinology 146, 4445–4455.

Saito, D., Takase, Y., Murai, H., and Takahashi, Y. (2012). The dorsal aorta initiates a molecular cascade that instructs sympatho-adrenal specification. Science 336, 1578–1581.

Shao, Y.W., Wood, G.A., Lu, J., Tang, Q.L., Liu, J., Molyneux, S., Chen, Y., Fang, H., Adissu, H., McKee, T., et al. (2019). Cross-species genomics identifies DLG2 as a tumor suppressor in osteosarcoma. Oncogene 38, 291–298.

Spitz, R., Hero, B., Ernestus, K., and Berthold, F. (2003). FISH analyses for alterations in chromosomes 1, 2, 3, and 11 define high-risk groups in neuroblastoma. Med. Pediatr. Oncol. 41, 30–35.

Srivatsan, E.S., Ying, K.L., and Seeger, R.C. (1993). Deletion of chromosome 11 and of 14q sequences in neuroblastoma. Genes Chromosomes Cancer 7, 32–37.

Subramanian, A., Tamayo, P., Mootha, V.K., Mukherjee, S., Ebert, B.L., Gillette, M.A., Paulovich, A., Pomeroy, S.L., Golub, T.R., Lander, E.S., and Mesirov, J.P. (2005). Gene set enrichment analysis: a knowledge-based approach for interpreting genome-wide expression profiles. Proc. Natl. Acad. Sci. USA 102, 15545–15550.

Suomi, T., Seyednasrollah, F., Jaakkola, M.K., Faux, T., and Elo, L.L. (2017). ROTS: an R package for reproducibility-optimized statistical testing. PLOS Comput. Biol. 13, e1005562.

Trochet, D., Bourdeaut, F., Janoueix-Lerosey, I., Deville, A., de Pontual, L., Schleiermacher, G., Coze, C., Philip, N., Frébourg, T., Munnich, A., et al. (2004). Germline mutations of the paired-like homeobox 2B (PHOX2B) gene in neuroblastoma. Am. J. Hum. Genet. 74, 761–764.

Umapathy, G., Guan, J., Gustafsson, D.E., Javanmardi, N., Cervantes-Madrid, D., Djos, A., Martinsson, T., Palmer, R.H., and Hallberg, B. (2017). MEK inhibitor trametinib does not prevent the growth of anaplastic lymphoma kinase (ALK)-addicted neuroblastomas. Sci. Signal. 10, eaam7550.

van Groningen, T., Koster, J., Valentijn, L.J., Zwijnenburg, D.A., Akogul, N., Hasselt, N.E., Broekmans, M., Haneveld, F., Nowakowska, N.E., Bras, J., et al. (2017). Neuroblastoma is composed of two super-enhancer-associated differentiation states. Nat. Genet. 49, 1261–1266.

Vivancos Stalin, L., Gualandi, M., Schulte, J.H., Renella, R., Shakhova, O., and Mühlethaler-Mottet, A. (2019). Expression of the Neuroblastoma-Associated ALK-F1174L Activating Mutation During Embryogenesis Impairs the Differentiation of Neural Crest Progenitors in Sympathetic Ganglia. Front. Oncol. 9, 275.

von Holst, A., Rodriguez-Tébar, A., Michaille, J.J., Dhouailly, D., Bäckström, A., Ebendal, T., and Rohrer, H. (1995). Retinoic acid-mediated increase in TrkA expression is sufficient to elicit NGF-dependent survival of sympathetic neurons. Mol. Cell. Neurosci. 6, 185–198.

Wezel, E.M.v., Zogchel, L.M.J.v., Wijk, J.v., Timmerman, I., Vo, N.-K., Zappeij-Kannegieter, L., deCarolis, B., Simon, T., Noesel, M.M.v., Molenaar, J.J., et al. (2019). Mesenchymal Neuroblastoma Cells Are Undetected by Current mRNA Marker Panels: The Development of a Specific Neuroblastoma Mesenchymal Minimal Residual Disease Panel. JCO Precis. Oncol. https://doi.org/10.1200/PO.18.00413.

Wieczorek, A., and Balwierz, W. (2015). The Role of Id2 Protein in Neuroblastoma in Children. Pathol. Oncol. Res. 21, 999–1004.

Wiśniewski, J.R., Zougman, A., Nagaraj, N., and Mann, M. (2009). Universal sample preparation method for proteome analysis. Nat. Methods 6, 359–362.

Woods, D.F., and Bryant, P.J. (1991). The discs-large tumor suppressor gene of Drosophila encodes a guanylate kinase homolog localized at septate junctions. Cell 66, 451–464.

Yang, S., Zheng, J., Xiao, X., Xu, T., Tang, W., Zhu, H., Yang, L., Zheng, S., Dong, K., Zhou, G., and Wang, Y. (2015). SOX2 promotes tumorigenicity and inhibits the differentiation of I-type neuroblastoma cells. Int. J. Oncol. 46, 317–323.

STAR★METHODS

KEY RESOURCES TABLE

REAGENT or RESOURCE	SOURCE	IDENTIFIER
Antibodies		
pALK (Y1604)	Cell Signaling Technology	Cat#3341L; RRID:AB_331047
DLG2	Cell Signaling Technology	Cat# 19046S; RRID:AB_2798811
pAKT(S473)	Cell Signaling Technology	Cat# 4060S; RRID:AB_2315049
phospho-p44/42 MAPK (Erk1/2)	Cell Signaling Technology	Cat# 4377L; RRID:AB_331775
α-Tubulin	Cell Signaling Technology	Cat# 2125S; RRID:AB_2619646
MAP2	Cell Signaling Technology	Cat# 8707; RRID:AB_2722660
AKT	Cell Signaling Technology	Cat#9272; RRID:AB_329827
SP1	Cell Signaling Technology	Cat# 9389S; RRID:AB_11220235
TrkA	Cell Signaling Technology	Cat# 2510S; RRID:AB_2797602
ERK1/2	BD Biosciences	Cat# 610124; RRID:AB_397530
Goat anti-Rabbit IgG (H+L) Cross-Adsorbed Secondary Antibody, HRP	Thermo Fisher Scientific	Cat# G-21234; RRID:AB_2536530
Goat anti-Mouse IgG (H+L) Cross-Adsorbed Secondary Antibody, HRP	Thermo Fisher Scientific	Cat# G-21040; RRID:AB_2536527
panALK	Chand et al., 2013	N/A
NEFH	Abcam	Cat#ab8135; RRID:AB_306298
Biological Samples		
Human neuroblastoma tumor and corresponding blood	Isolated from patients. This paper	N/A
Chemicals, Peptides, and Recombinant Proteins		
Power SYBR Green master mix	Thermo Fisher Scientific	Cat#4368577
lorlatinib	Selleckchem	Cat#S7536
Trametinib	Selleckchem	Cat#S2673
BEZ235	Selleckchem	Cat#S1009
Betulinic acid	Selleckchem	Cat#S3603
Puromycin	Thermo Fisher Scientific	Cat#A1113803
Doxycycline	Takara	Cat#631311
13-cis Retinoic acid	Selleckchem	Cat#S1379
ECL Prime Western Blotting System	Merck	Cat#GERPN2232
SuperSignal West Femto Maximum Sensitivity Substrate	Thermo Fisher Scientific	Cat#34095
Lipofectamine RNAiMAX	Thermo Fisher Scientific	Cat#13778075
Lysis Buffer A	Cell Signaling Technology	Cat#38191S
Critical Commercial Assays		
iScript cDNA Synthesis Kit	Biorad	Cat#1708890
Solution 3 DAPI	Chemometec	Cat#910-3003
ReliaPrep RNA Miniprep Systems	Promega	Cat#Z6011
DNeasy Blood & Tissue Kit	QIAGEN	Cat#69504
TruSeq DNA PCR-free	Illumina	Cat#20015963
Cytoscan HD array	Affymetrix	Cat#901835
Deposited Data		
Human reference genome NCBI build 37, GRCh37(hg19)	Genome Reference Consortium	https://www.ncbi.nlm.nih.gov/projects/genome/assembly/grc/human/
SweGen Variant Frequency dataset	SweGen project	https://swefreq.nbis.se/

Continued

REAGENT or RESOURCE	SOURCE	IDENTIFIER
Raw RNA-Seq data	This paper	ArrayExpress: E-MTAB-8657
Raw proteomics data	This paper	PRIDE: PXD017946
Processed data	This paper	Zenodo: 10.5281/zenodo.3692759
Experimental Models: Cell Lines		
SK-N-BE(2)	ATCC	Cat#CRL-2271
SH-SY5Y	ATCC	Cat#CRL-2266
SK-N-SH	ATCC	Cat#HTB-11
SK-N-AS	ATCC	Cat#CRL-2137
CLB-GA	Centre Leon Berard, France, Prof V. Combaret.	N/A
CLB-GE	Centre Leon Berard, France, Prof V. Combaret	N/A
Experimental Models: Organisms/Strains		
Mouse: Female BALB/cAnNRj-Foxn1nu	Janvier labs	N/A
Oligonucleotides		
Primer:DLG2 forward: CCCAGG TCTCTGGAACCTCT	This paper	N/A
Primer:DLG2 reverse: TGCTCGAT CATAGGTTTTCTTG	This paper	N/A
Primer: SP1 forward: CTATAGC AAATGCCCCAGGT	This paper	N/A
Primer:SP1 reverse: TCCACCTGCTGTGTCATCAt	This paper	N/A
Primer: SP1-wt probe forward: Biosg/ GCTGGTCCGGGGTTTGGA	This paper	N/A
Primer: SP1-wt probe reverse: /Biosg/TACCACTTC GGATTTCCGCCTA	This paper	N/A
Primer: Ctrl probe forward: /Biosg/ATGTCGCC ATCCACTCTAAAGT	This paer	N/A
SP1 siRNA #2	Thermo Fisher Scientific	Cat# AM16708; ID:116547
SP1 siRNA #3	Thermo Fisher Scientific	Cat#AM1670; ID:143158
Table S4, Supplemental primer table	This paper	N/A
Recombinant DNA		
pLenti-C-mGFP-P2A-Puro	Origene	Cat#RC227175L4
pLenti-DLG2-C-mGFP-P2A-Puro	Origene	Cat#RC227175L4V
pLVX-TRE3G	Takara	Cat#631187
pLVX-TET3G	Takara	Cat#631187
SP1(NM_138473.3) ORF Clone	Genscript	Cat#OHu18205D
SMARTvector Inducible DLG2 mCMV-TurboGFP shRNA (shDLG2 #1)	Horizon	Cat#V3SH7669-225727921
SMARTvector Inducible DLG2 mCMV-TurboGFP shRNA (shDLG2 #2)	Horizon	Cat#V3SH7669-227736101
SMARTvector Inducible Non-targeting Control mCMV/TurboGFP (shCtrl)	Horizon	Cat#VSC6570
Software and Algorithms		
Image Studio Lite software ver. 5.2	LI-COR	N/A
CHIPbase	N/A	http://rna.sysu.edu.cn/chipbase
R2: Genomics Analysis and Visualization Platform	AMC: Oncogenomics	https://hgserver1.amc.nl/cgi-bin/r2/main.cgi

(Continued on next page)

Continued

REAGENT or RESOURCE	SOURCE	IDENTIFIER
NucleoView Software	Chemometec	N/A
IncuCyte Software (v2019A)	Essen bioscience	N/A
Sentieon Genomic Tools	Sentieon Inc.	https://www.sentieon.com/products/
Canvas v1.38.0.1554	Roller et al., 2017 (https://doi.org/10.1093/bioinformatics/btw163)	https://github.com/Illumina/canvas
Manta v1.1.1	Chen et al., 2016 (https://doi.org/10.1093/bioinformatics/btv710)	https://github.com/Illumina/manta
ChAS	Affymetrix	http://www.affymetrix.com/support/technical/byproduct.affx?product=chas
CNAG 3.0	Nannya et al., 2005, (DOI: 10.1158/0008-5472.CAN-05-0465)	http://www.genome.umin.jp/CNAG_DLpage/CNAG_top.html
Hisat2	Kim et al., 2015	https://daehwankimlab.github.io/hisat2/
HTSeq	Anders et al., 2015	https://htseq.readthedocs.io/en/master/
DESeq2	Love et al., 2014	https://bioconductor.org/packages/release/bioc/html/DESeq2.html
ROTS	Suomi et al., 2017	https://bioconductor.org/packages/release/bioc/html/DESeq2.html https://bioconductor.org/packages/release/bioc/html/ROTS.html
Other		
Analysis of RNA-Seq and Proteomics data	This paper	Zenodo: 10.5281/zenodo.3982587

RESOURCE AVAILABILITY

Lead contact
Further information and requests for resources and reagents should be directed to and will be fulfilled by the Lead Contact Bengt Hallberg (bengt.hallberg@gu.se)

Materials Availability
Plasmid generated in this study can be made available upon request to the Lead Contact.

Data and Code Availability
Datasets and codes generated during this study are available at repositories indicated in the Key Resources Table.

EXPERIMENTAL MODEL AND SUBJECT DETAILS

Cell culture, cell lysis and western blot
All neuroblastoma cell lines were cultured in RPMI-1640 medium supplemented with 10% fetal bovine serum (FBS) and 1% penicillin and streptomycin at 37°C, 5% CO_2, 95% humidity. CLB-GE, CLB-GA, SK-N-BE(2), SH-SY5Y and SK-N-AS NB cell lines are described. SH-SY5Y, SK-N-BE(2), SK-N-AS and SK-N-SH were purchased from ATCC. CLB-GE and CLB-GA kindly provided by Dr. Valerie Combaret, Centre Leon Berard, France. Cells were regularly tested for mycoplasma using Eurofins mycoplasma testing plateform. Cells were recently authenticated (CLB-GE, CLB-GA and SK-NAS cells) by Tommy Martinsson, described in Umapathy et al. (2017).

Human patients
Neuroblastoma tumor samples and normal whole blood were collected from Swedish patients after either written or verbal informed consent was obtained from parents/guardians according to permits (registration numbers 03/736 and 09/1369) approved by the local ethics committee at Karolinska Institutet and Karolinska University Hospital.

Mouse models/animals
Female BALB/cAnNRj-Foxn1nu mice (Janvier Labs, France) 4-6 weeks old were group-housed in individually ventilated cages with access to irradiated standard chow and water *ad libitum* in a 12:12 light-dark cycle. The mice were randomly assigned to an

experimental group after 1 week of acclimatization at the facility. All experimental procedures and protocols were performed in accordance with the Regional Animal Ethics Committee approval, Jordbruksverket (01890-2018).

METHOD DETAILS

Immunoblotting

Cells were seeded, cultured overnight, and then treated for the indicated time points with the indicated inhibitors as outlined in figures. Whole cell lysates were collected in RIPA lysis buffer. Protein concentration was determined using the Pierce BCA Protein Assay Kit (Thermo Scientific) prior to boiling at 95°C for 5 minutes. Protein samples were subjected to 7.5% or 8.5% SDS polyacrylamide gel electrophorysis (PAGE), transferred to polyvinylidene difluoride membranes (Millipore) and immunoblotted with primary antibodies overnight at 4°C. Primary antibodies used, including ALK (Chand et al., 2013), are indicated in each figure. Secondary antibodies were used at a dilution of 1:5000 and incubated with shaking at room temperature for 1 hour. ECL prime western blotting detection reagent (Amersham,GE) was used. For endogenous DLG2 blots SuperSignal west femto maximum sensitivity substrate (Thermo Scientific) was used. Blots were scanned and analyzed using the Odyssey Imaging System and software (LI-COR). The primary antibodies, inhibitors and other chemicals used are described in the Key Resources Table.

Plasmid cloning and lentivirus

pLenti-DLG2-mGFP and pLenti-mGFP lentiviral particles were purchased from Origene Technologies. SK-N-BE(2). SMARTvector inducible non-targeting control, shCtrl, DLG2 shRNA; shDLG2 #1and shDLG2 #2 lentiviral particles were purchased from Horizon and described in the Key Resources Table. SP1(NM_138473.3) ORF cloned into pcDNA3.1 by, and ordered from, Genscript. The SP1 ORF was then subcloned into pLVX-TRE3G (Takara) lentiviral vector using infusion HD cloning (Takara) to form pLVX-TRE3G-SP1-c-Flag vector. Lentivirus supernatant was produced in HEK293T cells using pLVX-TRE3G-SP1-c-Flag vector and Lenti-X Packaging Single Shot reagent Xfect Transfection Reagent premixed with an optimized formulation of Lenti-X lentiviral packaging plasmids (Takara), and manufacturers protocol was followed. NB cell lines were transduced with respective lentiviral particles and corresponding stables cell lines were established as indicated in the figures. Transduced cells were selected with 1 μg/ml of puromycin to establish stable cell lines.

Cell proliferation, cell cycle and differentiation assays

Cells (6000 – 8000 cells/well) were seeded in triplicates into wells of 96-well plates (Eppendorf) and cultured in RPMI, supplemented with 10% FBS, overnight at 37°C in incucyte S3 (Essen BioScience). Cell growth/proliferation was recorded inside the incucyte by scanning the cells at 12 hours interval for 5 days. Cell percentage confluency was determined for each scan using incucyte S3 software (Essen BioScience). The normalized cell growth data was then imported to Graphpad Prism 7 to plot cell proliferation curves. The experiment was repeated three independent times.

For cell cycle analyses, cells (2.5×10^5 cells/well) were seeded and cultured RPMI, supplemented with 10% FBS for 48 hours. The cells were then harvested and rinsed with PBS, followed by ethanol fixation for 3 hours at 4°C. Cell cycle analysis was carried out using NucleoCounter NC-3000 (Chemometec) and manufacture's protocol, Fixed-Cell-Cycle-DAPI-Assay, was followed. Briefly, fixed cells were resuspended in solution 3 DAPI (1 μg/ml DAPI, 0.1% Triton X-100, in PBS) and incubated for 5 minutes at 37°C. Cells were then loaded unto NC-Slide A2 and scanned in NucleoCounter NC-3000. Cell cycle data was analyzed using plot manager in NucleoView NC-3000 software. Each experiment was repeated three independent times.

For differentiation assays, 50,000 to 60,000 cells were seeded in 6-well plates and cultured overnight and treated with retinoic acid (RA) (10 μM) or NGF (100 ng/ml) for indicated periods. Doxycycline was added on same day, where needed, when cells were seeded in 6-well plates, i.e at least 18 hours prior to RA treatment. Cells were considered as differentiated when a neurite projecting from a cell was at least 1.5 times the size of the cell body. At least 200 cells were counted in at least 4 random fields under microscope and the number of differentiated cells noted and calculated for percentage differentiation and graphs plotted with graphpad prism. Differentiated cells were photographed using Olympus CK40 microscope mounted with Olympus DP12 camera (Olympus Optical, Japan). Results are mean of at least three independent biological replicates.

RNA extraction and Quantitative PCR

To determine transcriptional responses of *DLG2* under different conditions, RNA extraction was done by ReliaPrep RNA Miniprep Systems (Promega) and cDNA was synthesized by iScript cDNA synthesis kit (Biorad). Quantitative PCR was performed on StepOnePlus Real-Time PCR Systems using Power SYBR® Green master mix and following primers presented in Key Resources Table and Table S4.

Nuclear extract isolation and DNA probe pulldown assay

Genomic DNAwas extracted from neuroblastoma cell line (SH-SY5Y) using DNAeasy Blood and Tissue kit (QIAGEN). CHIPbase (http://rna.sysu.edu.cn/chipbase) online tool predicted SP1 binding locus (chr11:85628043..85628782) located within 1 kilobase pair upstream of *DLG2* transcriptional start site. Biotinylated primers were ordered from Integrated DNA Technologies (IDT, Coraville, IA). SP1-wt probe (571 bp) spanning the predicted SP1 binding locus (chr11:85628043..85628782), was amplified from the extracted

genomic DNA using biotinylated primers. Control probe (ctrl) (628 bp) was amplified from random sequence within the DLG2 gene. The SP1binding locus was predicted to contain two SP1 motifs and these motifs were deleted in SP1-wt probe to form SP1 mutant probe (SP1-mut) (506 bp) using non-biotinylated primers. Primers used are outlined in the Key Resources Table.

For nuclear lysate extraction, cells were washed with ice-cold PBS and cell membrane was lysed using cell membrane lysis buffer A (Cell Signaling Technology) containing protease inhibitor cocktail (Cell Signaling Technology). Lysate was centrifuged at 9000 x g for 3 minutes at 4 °C and nuclear pellet was collected and washed once with 1 mL of buffer A. Nuclear pellet was resuspended in 0.5 to 1 mL buffer B (20mM HEPES, 100 mM KCl, 0.2 mM EDTA, 8% glycerol, pH 7.2) and sonicated on ice for 7 cycles (30 s ON, 40 s OFF, 100% amplitude) (Sonicator-FB120, Fisher Scientific, PA, USA). Nuclear suspension was centrifuged for 5 mins at 9000 x g and supernatant was collected and frozen at −80 °C. Protein concentration was measured by Pierce BCA protein assay kit (Thermo Fisher Scientific, Sweden).

For DNA probe pulldown assay, nuclear extract (50 μg to 100 μg) was mixed with 40 μl Dynabeads MyOne streptavidin C1 (Thermo Fisher Scientific, Sweden), 4 μg of biotinylated SP1-wt or ctrl DNA probes and diluted with PBS to 500 μl volume, followed by incubation at 4 °C for 90 minutes. In competition assay, nuclear extract was incubated with 15 μg of either non-biotinylated SP1-wt or SP1-mut probes for 2 hours prior to incubation with biotinylated 4 μg SP1-wt probe. Dynabeads were washed at least 5 times with 1 mL ice-cold PBS, with 5 minutes rotation per wash at 4 °C. Thereafter, 60 μl of 2X SDS sample buffer was added to beads, vortexed and heated at 95 °C for 5 minutes. Sample was subjected to PAGE and immunoblotted with SP1 antibody.

Mouse xenografts
Female BALB/cAnNRj-Foxn1nu mice (Janvier Labs, France) 4-6 weeks old were housed with access to food and water *ad libitum* in a 12:12 light-dark cycle. The animals were allowed to acclimatize for 1 week prior to being subcutaneously injected into the left flank with 2.5×10^6 SK-N-AS-GFP or SK-N-AS-DLG2 cells in serum-free medium mixed with Matrigel Matrix at a ratio of 1:1. The total injection volume was 100 μL. Tumor size was measured by caliper and the volume calculated by the following equation: V = (p/6) × L × W2 (V, volume; p, pi; L, length; W, width). The tumors were excised and weighed at the end of the experiment. All experimental procedures and protocols were performed in accordance with the Regional Animal Ethics Committee approval, Jordbruksverket (01890-2018).

RNA-Seq data analysis
RNA-seq reads were aligned to the human GRCh38 reference genome using hisat2 (Kim et al., 2015). The average alignment efficiency was 93.2%. Genes were annotated using GENCODE v29 (Harrow et al., 2012) and quantified using HTSeq (Anders et al., 2015). Only coding genes were used for further analysis. Differential gene expression was determined using DESeq2 (Love et al., 2014). Genes were considered differentially expressed if their absolute log2 fold change values were above 2 at false discovery rate (FDR)-adjusted P values below 0.01.

Differential expression heatmaps were constructed using the R gplots package. Hierarchical clustering was performed using the complete-linkage method and the Euclidean distance function (default settings). Only genes that were differentially expressed in minimal one of the analyzed conditions were considered.

ADRN and MES signature genes were derived from Van Groningen et al. (van Groningen et al., 2017). Within each sample, the rank percentile of an individual gene's expression value was used to define a gene score. The ADRN and MES gene signature score was then defined as the mean gene score of all ADRN and MES signature genes respectively.

A gene set enrichment analysis (GSEA) was performed to find gene ontology (GO) term enrichments and to predict TFs responsible for the observed differential expression. GSEA was performed using Fisher's exact test followed by false discovery rate (FDR) correction using the Benjamini-Hochberg method (Benjamini and Hochberg, 1995). Gene Ontology (GO) information was downloaded from the Molecular Signatures Database v6.2 (Subramanian et al., 2005) and transcription factor target information was derived from RegNetwork (Liu et al., 2015), downloaded from http://www.regnetworkweb.org/. Only TFs that were expressed in the analyzed samples were considered.

Proteomic Tandem Mass Tag labeling and LC-MS/MS analysis
For proteomic sample preparation, SH-SY5Y-GFP and SH-SY5Y-DLG2 cells were seeded and treated with either DMSO or retinoic acid (10 μM) for 24 hr. Cells were harvested and washed with PBS. Cell pellets were homogenized using a FastPrep®-24 instrument (MP Biomedicals, https://www.mpbio.com) with Lysing Matrix D for five repeated cycles (speed 6.5 m/s, 40 s/cycle) in 200 μl of the buffer containing 2% sodium dodecyl sulfate and 50mM triethylammonium bicarbonate (TEAB). Samples were centrifuged at 16 000 g for 10 min and the supernatants were transferred into clean tubes. Protein concentration of the lysates was determined using Pierce BCA Protein Assay Kit (Thermo Scientific) and the Benchmark Plus microplate reader (BIO-RAD) with bovine serum albumin (BSA) solutions as standards.

Prior to TMT labeling, samples were digested with trypsin using the filter-aided sample preparation (FASP) method (Wiśniewski et al., 2009). Briefly, 30 ug from each sample was reduced with 100 mM dithiothreitol at 60°C for 30 min, transferred to 30 kDa MWCO Pall Nanosep centrifugation filters (Sigma-Aldrich), washed several times with 8 M urea and once with digestion buffer prior to alkylation with 10 mM methyl methanethiosulfonate in digestion buffer for 30 min. Digestion was performed in 50 mM TEAB, 1% sodium deoxycholate (SDC) buffer at 37°C by addition of 0.3 μg Pierce MS grade Trypsin (Thermo Fisher Scientific) and incubated

overnight. An additional portion of trypsin was added and incubated for another three hours. Peptides were collected by centrifugation, and labeled using TMT 11-plex isobaric mass tagging reagents (Thermo Scientific) according to the manufacturer instructions. After pooling of the TMT set, SDC was removed by acidification with 10% TFA. The proteins were pre-fractionated into 40 fractions by basic reversed-phase chromatography (bRP-LC) using a Dionex Ultimate 3000 UPLC system (Thermo Fisher Scientific). Peptide separation was performed using a reversed-phase XBridge BEH C18 column (3.5 μm, 3.0x150 mm, Waters Corporation) and a linear gradient from 3% to 40% acetonitrile in 10 mM ammonium formate buffer at pH 10.00 over 17 min, followed by an increase to 90% acetonitrile over 5 min. The fractions were concatenated into 20 fractions, dried and reconstituted in 3% acetonitrile, 0.2% formic acid.

For LC-MS/MS analysis, peptide fractions were analyzed on an Orbitrap Fusion Tribrid mass spectrometer interfaced with Easy-nLC1200 liquid chromatography system (both Thermo Fisher Scientific). Peptides were trapped on an Acclaim Pepmap 100 C18 trap column (100 μm x 2 cm, particle size 5 μm, Thermo Fisher Scientific) and separated on an in-house packed analytical column (75 μm x 30 cm, particle size 3 μm, Reprosil-Pur C18, Dr. Maisch) using a linear gradient from 5% to 35% B over 75 min followed by an increase to 100% B for 5 min, and 100% B for 10 min at a flow of 300 nL/min. Solvent A was 0.2% formic acid in water and solvent B was 80% acetonitrile, 0.2% formic acid. MS scans were performed at a resolution of 120,000, m/z range 380-1380. MS/MS analysis was performed data-dependent, with top speed cycle of 3 s for the most intense doubly or multiply charged precursor ions. Most intense precursors were fragmented in MS2 by collision induced dissociation (CID) at a collision energy of 35 with a maximum injection time of 50 ms, and detected in the ion trap followed by multinotch (simultaneous) isolation of the top 10 MS2 fragment ions, with m/z 400-1400, selected for fragmentation (MS3) by higher-energy collision dissociation (HCD) at 65% and detection in the Orbitrap at a resolution of 50,000 and m/z range of 100-500. Precursors were isolated in the quadrupole with an isolation window of 0.7 m/z and a dynamic exclusion within 10 ppm during 60 s was used for m/z-values already selected for fragmentation.

The data files for the TMT set were merged for identification and relative quantification using Proteome Discoverer version 2.2 (Thermo Fisher Scientific). The search was performed by matching against the *Homo sapiens* Swissprot Database (version November 2017, Swiss Institute of Bioinformatics, Switzerland) using Mascot 2.5 (Matrix Science) with a precursor mass tolerance of 5 ppm and fragment mass tolerance of 0.6 Da. Tryptic peptides were accepted with zero missed cleavage, variable modifications of methionine oxidation and fixed cysteine alkylation; TMT-label modifications of N-terminal and lysine were selected. Percolator was used for the validation of identified proteins and the quantified proteins were filtered at 1% FDR and grouped by sharing the same sequences to minimize redundancy. TMT reporter ions were identified in the MS3 HCD spectra with 3 mmu mass tolerance, and the TMT reporter intensity values for each sample were normalized on the total peptide amount. Only peptides unique for a given protein were considered for quantification.

Differential protein expression was determined using the R *ROTS* package (Love et al., 2014; Suomi et al., 2017). Proteins were considered differentially expressed if their absolute log2 fold change values were above 1 at false FDR-adjusted *P value*s below 0.01.

SNP microarray analysis and whole genome sequencing

Genomic profiling on human NB tumors was performed with high density Affymetrix single nucleotide polymorphism (SNP) microarrays as described earlier (Carén et al., 2010). For primary data analysis, the GDAS software (Affymetrix) was used while genomic profiles and determination of amplicon boundaries were performed using either Chromosome Analysis Suite (ChAS) (Affymetrix) or Copy Number Analyzer for Affymetrix GeneChip Mapping arrays (CNAG 3.0) (Nannya et al., 2005). The genomic position of endpoints was determined as the position of the first marker located outside of the amplified region according the UCSC hg19 assembly.

Whole genome sequencing (WGS) was performed on tumor DNA and corresponding constitutional DNA extracted from blood for 8 neuroblastoma patients with intragenic *DLG2* aberrations aiming for at least an average coverage of 60X for tumor libraries and 30X for constitutional DNA using Illumina instrumentation (Illumina, San Diego, CA, USA) at Clinical Genomics, SciLife Laboratories, Stockholm, Sweden. Mapping to the human reference genome hg19, removal of read duplicates, realignment around InDels and basescore-recalibration and variant calling was carried out using the Sentieon suite of bioinformatics tools (Sentieon Inc, Mountain View, CA). The Canvas tool (version 1.38.0.1554) (Roller et al., 2016) was used to call copy number alterations (CNA), where gains and losses of genomic regions as well as LOH-regions were identified using read depth coverage in combination with SNV b-allele frequencies. For calling of germline and somatic CNVs the SmallPedigree-WGS and Somatic-WGS algorithms of Canvas was used respectively. Calling of somatic structural variants (SV) were done using the Manta tool (version 1.1.1) (Chen et al., 2016) that applies information of soft clipped read ends, disjointed read-pairs and read-pair orientation for identification of larger structural variation (deletions, duplications, inversions and translocations). Calls from the constitutional DNA were supplied to filter out germline variation and artifacts caused by problematic regions, in addition, further filtering and removal were also done based on presence in the Swe-Gen Variant Frequency dataset (https://swefreq.nbis.se/) or in our in-house set of normal controls.

QUANTIFICATION AND STATISTICAL ANALYSIS

Graphs were generated and statistical analysis was performed using GraphPad Prism 8.01 or the R statistical package (v. 3.5). Western blots were quantified using Image studio lite software (LI-COR). The number of biological replicates, (at least n = 3), are indicated in each figure. Details on the statistical tests used in this study are reported in the respective sections and figure captions.